Bioinspired gelatin/bioceramic composites loaded with bone morphogenetic protein-2 (BMP-2) promote osteoporotic bone repair

Echave, M. C.; Erezuma, I.; Golafshan, N.; Castilho, M.; Kadumudi, F. B.; Pimenta-Lopes, C.; Ventura, F.; Pujol, A.; Jimenez, J. J.; Camara, J. A.

Total number of authors:
25

Published in:
Materials Science and Engineering C

Link to article, DOI:
10.1016/j.msec.2021.112539

Publication date:
2022

Document Version
Peer reviewed version

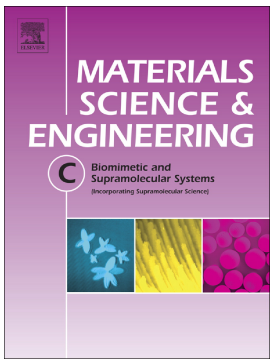

Bioinspired gelatin/bioceramic composites loaded with bone morphogenetic protein-2 (BMP-2) promote osteoporotic bone repair

M.C. Echave, I. Erezuma, N. Golafshan, M. Castilho, F. Babu Kadumudi, C. Pimenta-Lopes, F. Ventura, A. Pujol, J.J. Jimenez, J.A. Camara, R. Hernáez-Moya, L. Iturriaga, L. Sáenz Del Burgo, I. Lloro, M. Azkargorta, F. Elortza, R. Lakshminarayanan, Taleb H. Al-Tel, P. García-García, R. Reyes, A. Delgado, C. Évora, J.L. Pedraz, A. Dolatshahi-Pirouz, G. Orive

PII: S0928-4931(21)00679-2

DOI: https://doi.org/10.1016/j.msec.2021.112539

Reference: MSC 112539

To appear in: *Materials Science & Engineering C*

Received date: 31 May 2021

Revised date: 29 October 2021

Accepted date: 3 November 2021

Please cite this article as: M.C. Echave, I. Erezuma, N. Golafshan, et al., Bioinspired gelatin/bioceramic composites loaded with bone morphogenetic protein-2 (BMP-2) promote osteoporotic bone repair, *Materials Science & Engineering C* (2021), https://doi.org/10.1016/j.msec.2021.112539

Bioinspired gelatin/bioceramic composites loaded with bone morphogenetic protein-2 (BMP-2) promote osteoporotic bone repair

Echave MC[1,2], Erezuma I[1,3], Golafshan N[4,5], Castilho M[4,5,6], Babu Kadumudi F[7], Pimenta-Lopes C[8], Ventura F[8], Pujol A[9], Jimenez JJ[9], Camara JA[9], Hernáez-Moya R[1,2], Iturriaga L[1,2], Sáenz Del Burgo L[1,2,3], Lloro I[10], Azkargorta M[10], Elortza F[10], Lakshminarayanan R[11], Taleb H Al-Tel[12], García-García P[13], Reyes R[14,15], Delgado A[13,15], Évora C[13,15], Pedraz JL[1,2,3], Dolatshahi-Pirouz A[4,16,], Orive G[1,2,3,17,18,*]*

Affiliations

[1]NanoBioCel Group, Laboratory of Pharmaceutics, School of Pharmacy, University of the Basque Country (UPV/EHU), Paseo de la Universidad 7, 01006 Vitoria-Gasteiz, Spain.
[2]Biomedical Research Networking Centre in Bioengineering, Biomaterials and Nanomedicine (CIBER-BBN). Vitoria-Gasteiz, Spain.
[3]Bioaraba, NanoBioCel Research Group, Vitoria-Gasteiz, Spain.
[4]Regenerative Medicine Center, University Medical Center Utrecht, Utrecht, The Netherlands.
[5]Department of Orthopedics, University Medical Center Utrecht, Utrecht, The Netherlands.
[6]Department of Biomedical Engineering, Eindhoven University of Technology, Eindhoven, The Netherlands.
[7]Department of Health Technology, Technical University of Denmark, 2800 Kgs. Lyngby, Denmark.
[8]Departament de Ciències Fisiològiques, Universitat de Barcelona, IDIBELL, Hospitalet de Llobregat, Spain.
[9]Preclinical Imaging Platform, Vall d'Hebron Institute of Research, Barcelona, Spain.
[10]Proteomics Platform, CIC bioGUNE, BRTA (Basque Research and Technology Alliance), CIBERehd, ProteoRed-ISCIII, Bizkaia Science and Technology Park, Derio, Spain.
[11]Anti-Infectives Research Group, Singapore Eye Research Institute, Singapore.
[12]Sharjah Institute for Medical Research, University of Sharjah, Sharjah, United Arab Emirates; College of Pharmacy, University of Sharjah, Sharjah, United Arab Emirates.
[13]Department of Chemical Engineering and Pharmaceutical Technology, Universidad de La Laguna, 38200 La Laguna, Spain.
[14]Department of Biochemistry, Microbiology, Cell Biology and Genetics, Universidad de La Laguna, 38200 La Laguna, Spain.
[15]Institute of Biomedical Technologies (ITB), Center for Biomedical Research of the Canary Islands (CIBICAN), Universidad de La Laguna, 38200 La Laguna, Spain.
[16]Technical University of Denmark, DTU Health Tech, Center for Intestinal Absorption and Transport of Biopharmaceuticals, 2800 Kgs, Denmark; Radboud University Medical Center, Radboud Institute for Molecular Life Sciences, Department of Dentistry - Regenerative Biomaterials, Philips van Leydenlaan 25, 6525EX Nijmegen, the Netherlands.
[17]University Institute for Regenerative Medicine and Oral Implantology - UIRMI (UPV/EHU-Fundación Eduardo Anitua), Vitoria, Spain.
[18]Singapore Eye Research Institute, The Academia, 20 College Road, Discovery Tower, Singapore.

Corresponding Author

Gorka Orive: gorka.orive@ehu.es

NanoBioCel Group, Laboratory of Pharmaceutics, School of Pharmacy, University of the Basque Country (UPV/EHU), Paseo de la Universidad 7, 01006 Vitoria-Gasteiz, Spain.

ABSTRACT

There are currently several commercialized products approved by the Food and Drug Administration and the European Medicines Agency based on the use of recombinant human BMP-2 for the treatment of non-unions long fractures and spinal fusion. However, the adverse effects recorded with the use of BMPs suggest the need for drug delivery carriers that allow reducing the required doses and improve their cost-effectiveness. Herein, we have developed a new osteoconductive scaffold that reduces the required doses of BMP-2 for promoting bone regeneration in an osteoporotic defect model. The composite is, in brief, a gelatin-based 3D scaffold reinforced with either calcium sulfate or hydroxyapatite as an inorganic osteoconductive biomaterial. To this end, the organic/inorganic composite systems showed high hydration capacity and good *in vitro* degradability. The incorporation of 7.5% (m/v) ceramic compounds resulted in scaffolds with stiffer Young modulus (179 and 75 kPa for $CaSO_4$_7 and HA_7, respectively) than bare gelatin hydrogels (48 kPa). Studies with human bone-marrow derived mesenchymal stem cells (hBM-MSCs) revealed that the 3D scaffolds promote cell adhesion and proliferation along with osteogenic differentiation capabilities. Specifically, downregulation of stemness (*Nanog, Oct4*) genes and upregulation of osteogenic markers (*ALP, Col1a1, Fmod*) by two fold were observed over 10 days under basal culture conditions. Promisingly, the sustained *in vitro* release of BMP-2 observed from the porous reinforced scaffolds allowed us to address the critical-sized osteoporotic mice calvarial defects with a relatively low growth factor doses (600 ng BMP-2/scaffold) compared to conventional doses at 2-15 micrograms. Overall, this study demonstrates the promising potential of osteoconductive gelatin/calcium bioceramics

composites as osteogenic growth factors delivery carriers for bone-regeneration via ultra-low growth factor doses.

Graphical Abstract

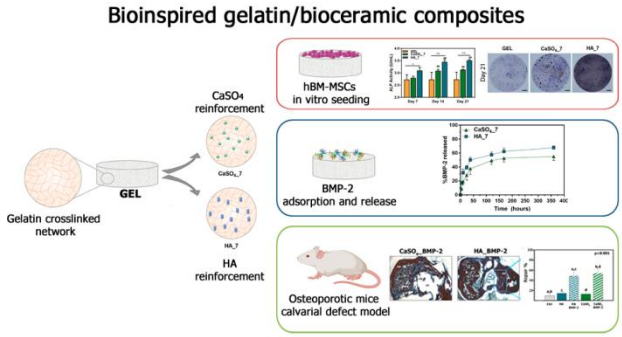

KEYWORDS: bone, bone morphogenetic protein -2, calcium sulfate, gelatin, hydroxyapatite, osteoporosis

1. Introduction

Osteoporosis is one of the most frequent bone disorders. It is characterized by the decrease in the bone mass and consequent deterioration of bone microstructure, which results in increased bone fragility and susceptibility to fracture [1]. It is estimated that more than 9 million osteoporotic fractures occur every year worldwide [2]. In adulthood the mass and volume of the bones remain constant because of the coordinated homeostasis of bone formation and resorption by osteoblast and osteoclasts respectively. Behind the pathophysiology of osteoporosis is the loss of bone turnover regulation, i.e. excess of bone resorption against bone formation [3]. The current treatment for osteoporosis consists of systemic administration of antiresorptive drugs (e.g. bisphosphonates) that inhibit osteoclasts activity, and anabolic agents (e.g. teriparatide) that promote bone formation by stimulating osteoblast activity. Importantly, it has been demonstrated that, during the development of this pathology, bone marrow derived mesenchymal stem cells (BM-MSCs) reduce their ability to differentiate into osteoblasts and increase their differentiation to adipogenic lineage [4]. Therefore, the poor osteogenic capacity due to the disruption of BM-

MSCs differentiation balance makes the repair of bone defects after an osteoporotic fracture particularly challenging.

The synergistic integration of therapeutically active growth factors and drug delivery platforms is a promising approach for the treatment of osteoporosis. Among the various growth factors, bone morphogenetic protein-2 (BMP-2), which belongs to the transforming growth factor β (TGF-β) superfamily, is one of the most studied [5]. Importantly, BMP-2 induces the osteogenic differentiation of MSC and osteoprogenitor cells during bone healing and formation [6]. What is more, it has been observed that BMP proteins are key growth factors in order to boost osteoinduction [7,8]. However, unfortunately, the administration of BMP-2 is complex and usually results in a therapeutic effect only via supra-physiological concentrations, which in turn can facilitate adverse reactions in the patient. For instance, concentrations of BMP-2 range from micrograms to tens of micrograms in rodents and up to tens of milligrams in human [9,10]. The development of systems that are intrinsically more osteoconductive with reduced dependence on BMP-2 to promote bone regeneration would address these problems and improve the osteogenic capabilities within the bone tissue engineering field [11]. These carriers would ideally allow not only the controlled release of the growth factor to customize its exposure at the site of injury, but provide the essential cues to promote the adhesion, proliferation and extracellular matrix deposition by host cells, which are already partially differentiated (e.g. preosteoblasts). To achieve this goal, bioinspired organic/inorganic composite systems that resemble the natural composition of bone tissue have extensively been proposed [12,13].

Gelatin, as a denatured form of collagen, is one of the main constituents of living bone. Thus, an interesting biomaterial to be used for the organic phase of the proposed composite systems. Its intrinsic ability to create polyion complexes with charged therapeutic agents has made this

biodegradable protein particularly fruitful biomaterial for biomedical applications [14]. On the other hand, calcium phosphate and calcium sulfate-based bioactive ceramics can stimulate bone formation and thereby potentially improve the osteoconductivity of the composite.

In the present study, we present a gelatin-based 3D scaffold to support the osteogenic commitment and the release of osteogenic BMP-2 growth factor by incorporating calcium ceramic compounds for osteoporotic bone tissue engineering purposes. For this aim, the gelatin network was enzymatically crosslinked and the therapeutic agent was loaded to the preformed scaffolds. Different ratios of calcium sulfate and hydroxyapatite (HA) were successfully incorporated into the matrices and the swelling, degradation and mechanical properties were evaluated. Furthermore, the analysis of the microstructure and chemical composition were evaluated. The biological performance of the developed scaffolds was assessed by culturing human bone-marrow derived mesenchymal stem cells (hBM-MSCs) on the scaffold surface and cellular adhesion, proliferation, viability and osteogenic differentiation capacity were determined. hBM-MSCs differentiation fate was assessed through the analysis of the expression levels of both stemness (*Nanog, Oct4*) and osteoblast-related genes (*Col1a1, Runx2, Fmod*) by RT-PCR assay. Finally, bone regenerative potential of the developed 3D scaffolds was investigated in osteoporotic mice critical-size calvarial defects.

2. Materials and Methods

2.1 Materials

Gelatin from bovine skin Type B (~ 225 g Bloom), calcium sulfate dihydrate, hydroxyapatite particles, Cell Counting Kit-8 (CCK-8), Triton X-100, collagenease P, bovine serum albumin (BSA), p-nitrophenyl phosphate (pNPP) and calf intestinal alkaline phosphatase (CIAP) were purchased from Sigma Aldrich, Spain. Microbial Transglutaminase (100 U/g) was kindly

supplied by Ajinomoto Foods Europe, France. Phosphate Buffered saline (PBS), Trypsin, fetal bovine serum (FBS), Penicillin-Streptomycin solution, Dulbecco's Modified Eagle Medium/Nutrient Mixture F-12 (DMEM/F12), Pierce™ BCA Protein Assay Kit, 4,6-diamidino-2-phenyindole dilactate (DAPI), AlexaFluor 488-phalloidin, LIVE/DEAD® kit and 5-bromo-4-chloro-3-indolyl phosphate/nitroblue tetrazolium (BCIP/NBT) were obtained from Fisher Scientific, Spain. Calcium Detection Kit was purchased from Abcam and TRIsure™ reagent from Bioline. Recombinant human bone morphogenetic protein -2 (rh-BMP-2) was purchased from GenScript and ELISA kit for rh-BMP-2 detection from Peprotech, UK.

2.2 Fabrication of 3D scaffolds

Enzymatically crosslinked gelatin-based 3D scaffolds were prepared by the freeze-drying technique. Initially, 1 g of gelatin from bovine skin was dissolved in 3mL distilled water under constant stirring at 40 ºC for 1 hour. Then, different concentrations (3.75, 7.5 and 15% (w/v)) of calcium sulfate salt or HA particles were mixed with gelatin in order to obtain different reinforced scaffolds with low, medium or high grade, respectively. These reinforced gelatin dispersions were mixed with the microbial transglutaminase enzyme solution at a 1.5:1 (v/v) ratio to reach the final scaffolds composition of 20% (w/v) gelatin and 20 U/g gelatin enzymatic activity. A scaffold without addition of reinforcement materials was also prepared for comparison. Afterward, the hydrogels were casted into polystyrene molds and punched out to obtain desirable sized cylindrical 3D scaffolds. These structures were immersed in ethanol 70% (v/v) for 15 minutes and thereafter two washings with PBS were performed, in order to discard any remaining ethanol. Subsequently, the samples were first frozen at -80 ºC, and freeze-dried after.

2.3 Swelling ratio and degradation profile

The swelling behavior of the gelatin-based scaffolds was determined in PBS at 37 ºC under constant shaking (300 rpm). The initial dry weight of each sample was measured and, then, scaffolds were immersed in PBS at 37 ºC. The wet weight of the samples at different time intervals (1, 2, 5, 10, 15 and 30 min, 1, 2, 7, and 24 hours and 6 days) were measured after removing the excess water from the surface. The swelling ratio was calculated following equation 1, where Ws is the weight of the wet sample and the Wo corresponds to the initial dry weight of the same sample.

[Eq. 1] Swelling Ratio = (Ws – Wo)/Wo

To study the stability of the samples under physiological conditions, both hydrolytic and enzymatic degradation tests were performed. For the hydrolytic degradation test, the samples were first immersed in PBS until swelling equilibrium was reached (2 hours) and weighed then. This value was considered as initial weight and the samples were immersed in PBS and maintained at 37 ºC during 9 days. At each time point, samples were taken out and the weight of each sample was recorded. The degradation rate was determined by the weight of the remaining matrices following equation 2, where Wi is the initial weight of the sample and the Wt corresponds to the weight of the sample at different time intervals.

[Eq. 2] Weight of scaffolds (%) = (Wt/Wi)*100

For the enzymatic degradation test, collagenase P solution at 0.02% (w/v) concentration was used to immerse the samples. In these case, when the samples were completely degraded the total protein and calcium content of the supernatants were determined by commercially available kits, following the instructions of the manufacturer.

2.4 Physicochemical characterization

2.4.1 Compressive mechanical properties

The compressive mechanical behavior of the developed scaffolds was analyzed by monotonic uniaxial unconfined compression, following a protocol described elsewhere [15]. A universal mechanical testing (Instron 5548) equipped with 50 N load cell was used. Prior to the test, the cylindrical samples were immersed in phosphate buffer saline (PBS) for 24 hours and the size of the scaffolds was measured prior to the compression (1mm height and 10 mm diameter).

Tests were performed at a rate of 1 mm/min, at room temperature. The Young modulus was determined from the slope of the engineered stress-strain curves in the 10-20% strain linear region. Same experimental settings were applied to measure at least six different samples per each composition.

2.4.2 Scanning Electron Microscopy (SEM) and Energy Dispersive X-ray Spectroscopy (EDAX) Analysis

In order to determine the porosity of the hydrogels SEM analysis were performed. SEM images were acquired with SEM Quanta FEG 250 Analytical ESEM instrument operating at an accelerating voltage 2 kV in high vacuum mode after gold sputtering the freeze dried hydrogels with 5 nm. ImageJ software was used to measure the pore size of the collected SEM images and average pore size was calculated from at least 40 measurements from each sample. EDAX analysis was performed with Oxford Instruments 80 mm^2 X-Max silicon drift detector connected to the SEM instrument after gold sputtering with 5 nm.

2.4.3 Fourier Transform Infrared Spectroscopy (FTIR) Analysis

The chemical composition of the lyophilized scaffolds was assessed by means of FTIR spectroscopy. FTIR spectra of the freeze-dried hydrogels were recorded on attenuated total reflection (ATR) mode using a PerkinElmer Spectrum 100 FTIR spectrophotometer with an ATR accessory after background subtraction. Spectra were recorded over the range of 4000-500

cm^{-1} with 16 scans at a resolution of 4 cm^{-1}. The collected spectra were baseline-corrected and normalized using PerkinElmer Spectrum software and the average of four spectra were used for the analysis.

2.4.4 X-ray Diffraction (XRD) Analysis

The XRD patterns of the freeze dried hydrogels were collected with a Huber G670 powder diffractometer in the 2θ range of 3 to 100° in steps of 0.005° using CuKα1 radiation (λ = 1.54056 Å) for 10 min. The data were collected in transmission mode from a rotating flat plate sample inclined 45° relative the primary beam.

2.5 In vitro release of bone morphogenetic protein – 2 (BMP-2)

The *in vitro* release of BMP-2 growth factor from the developed formulations was evaluated with 4 mm diameter scaffolds and Protein LoBind Eppendorf tubes. First, previously prepared and lyophilized scaffolds were loaded with 600 ng of BMP-2 as described in our previous paper [16] and they were incubated overnight for the protein adsorption. Afterward, a washing step with 1 mL of PBS was performed to remove the unbound protein fraction before the sampling phase was initiated. The *in vitro* release assay was performed at 37 ºC under mild orbital agitation and at each time point, all the volume of PBS in tubes was collected and replaced with fresh one. After collecting the last sample, the scaffolds were degraded with collagenase P solution in order to determine the amount of growth factor remaining in the scaffolds. All the samples were kept frozen until the determination of the BMP-2 concentration by commercial ELISA kit following the manufacturer´s guideline.

2.6 Biocompatibility study

The preliminary cellular compatibility of the scaffolds was assessed as described by Echave MC et al. [16], following the guideline ISO 10993 (Biological evaluation of medical devices

guideline: cytotoxicity on extracts and cytotoxicity by direct contact). Both the cytotoxicity produced by cell-scaffold direct interaction and the indirect toxicity of the scaffolds were determined by the evaluation of the cells metabolic activity trough the CCK-8 assay. The metabolic activity of cells without contact with scaffolds or the extracts was considered as 100% viability.

2.7 In vitro cell studies: human Bone-Marrow derived Mesenchymal Stem Cells (hBM-MSCs) seeding on the developed systems

2.7.1 hBM-MSC expansion and seeding

hBM-MSC were expanded in complete basal medium consisting of DMEM/F12 culture medium, supplemented with 10% (v/v) FBS and 1% (v/v) penicillin/streptomycin solution. Cells were cultured at 37 ºC in a humidified atmosphere with 5% CO_2 and the split of the cells was done when reached confluence. hBM-MSCs were used at passage 3-5 for all the cellular studies. Before the seeding of the cells on the top of the 3D systems, all the scaffolds were exposed to UV light for 15 minutes and hydrated with the basal culture medium. The hydrated scaffolds were placed in wells of the same size in ultra-low attachment microplates (Corning™ Costar™ Ultra-Low Attachment Microplates) and 10^5 hBM-MSC/scaffold in 30 µL of medium were seeded onto the surface of the scaffolds. These scaffolds were kept in the CO_2 incubator for 1.5 hours and then 1.5 mL of complete basal medium was added to each well. The culture medium was changed every 2-3 days during the experiments.

2.7.2 Live/dead viability assay

Cell viability at the enzymatically crosslinked gelatin-based substrates was evaluated using Live/Dead viability assay (Life Technologies) according to the manufacturer´s protocol. After 2 and 10 days of culture, three samples of each group (GEL, $CaSO_4$_7 and HA_7) were incubated

in calcein-AM/ethidium solution for 30 min and fluorescence micrographs were taken using inverted fluorescence microscope (Nikon TMS). Flow cytometry (MACSQuant Analyzer, Miltenyi Biotec) was used to quantify the viability of the cells seeded on the surface of the scaffolds at day 10. First, cells were detached from the scaffolds with trypsin-EDTA and dyed after with Live/Dead kit, following the guidelines.

2.7.3 Cell adhesion, proliferation and metabolic activity determination

Immunofluorescence staining was performed to study the adhesion and proliferation of hBM-MSCs cells on the scaffolds. The cell-seeded scaffolds were washed with PBS and fixed with 3.7% (v/v) formaldehyde for 10 min after 7 days of culture. The cells were permeabilized with 0.1% (v/v) Triton X-100 for 5 min and the blocking of the samples was performed with 1% (w/v) BSA for 30 min. The F-actin filaments were stained with 165 nM AlexaFluor 488-labelled phalloidin for 30 min at room temperature protected from light. After washing the samples with PBS three times, the nuclei were stained with 300 nM DAPI solution. The samples were observed under inverted fluorescence microscope (Nikon TMS).

The proliferation of hBM-MSCs on the 3D scaffolds was evaluated by means of metabolic activity determination following CCK-8 assay. The cell-seeded samples were rinsed with PBS after 2, 7 and 10 days of incubation and 350 µL of fresh medium containing 35 µL of CCK-8 kit reagent was added to each scaffold. The samples were incubated for 4 h at 37 ºC and the optical density of the generated formazan was measured by Tecan Infinite M2000 microplate reader.

2.7.4 Alkaline Phosphatase (ALP) activity and staining

The secretory form of ALP from the cells was evaluated spectrophotometrically during 3 weeks. The activity was evaluated by determining the hydrolysis of p-nitrophenyl phosphate by ALP at pH 9.3. A standard curve with calf intestinal ALP was prepared and 100 µL of pNPP at

0.2% (w/v) was added to each sample. The reaction was stopped with 50 µL of NaOH 3M and absorbance measured at 405 nm. Moreover, for the evaluation of the intracellular ALP activity of hBM-MSC seeded onto the scaffolds at the end of the assay, BCIP/NBT solution was used. After washing the scaffolds three times with PBS, the samples were covered with the solution and incubated protected from light at room temperature for 2 h. Then, the excess of the dye was discarded washing the scaffolds three times with PBS. The stained scaffolds were observed under bright field and imaged with a digital camera. Image J software was used for the analysis of the images and the area covered by the black-violet stained cells was determined by applying a threshold. The entire area of the scaffold was considered as 100%.

2.7.5 RNA Isolation and Real-Time Quantitative Reverse Transcriptase-Polymerase Chain Reaction (q-RT-PCR)

Total RNA was isolated from primary hBM-MSC using TRIsure reagent (Bioline, London, UK). 1 µg of total RNA was reverse transcribed into cDNA using the High-Capacity cDNA Reverse Transcription Kit (Applied Biosystems). Quantitative real-time PCR was performed using the SensiFAST Probe Hi-ROX Mix (Bioline) in an ABI Prism 7900 HT Fast Real-Time thermocycler. The genes were screened using Taqman 5′-nuclease probe method (Applied Biosystems) and all transcripts were normalized to the housekeeping gene TATA binding protein (Tbp). Fold-change expression was calculated using the $2^{-\Delta\Delta Ct}$.

2.8 In vivo evaluation of bone regeneration

2.8.1 Osteoporotic mice calvaria defect model

The animal experiments were carried out in conformity with the European Directive (2010/63/UE) on Care and Use of Animals in Experimental Procedures. In addition, the animal protocols were previously approved by the Ethics Committee for Animal Care of the University

of La Laguna. The surgeries were carried out under isoflurane anesthesia. The analgesia consisted in buprenorphine (0.01 mg/kg) by subcutaneous route before the surgeries and paracetamol (200 mg/kg) in the drinking water, for 3 days post-surgery. Furthermore, after recovery from the surgeries, animals were allowed free movement, food and water uptake. Experimental osteoporosis was induced to 20 female FVB mice, approximately 16 weeks old, by bilateral ovariectomy, via dorsal approach. Immediately after the surgery the mice received 3 mg/kg body weight of dexamethasone-21-isonicotinate (Deyanil Retard, Fatro Ibérica, Spain) administered subcutaneously once a week for up to 16 weeks. Then, the animals underwent a new surgery to create the bone defect and simultaneously the scaffolds were implanted. Briefly, the calvaria bone was exposed and a 4mm circular area was delimited with a biopsy punch. Then, a 4 mm circular trans-osseous defect was made with a trephine bur [17]. The scaffold was inserted in the defect and the skin was stapled. At 8 weeks post-implantation, animals were sacrificed by CO_2 inhalation and the defect area was extracted.

2.8.2 Histology, histomorphometry and immunohistochemistry analysis

The extracted samples were prepared for histological analysis as previously described [18]. Briefly, samples were fixed in paraformaldehyde 4% solution first, decalcified in Histofix® Decalcifier (Panreac, Barcelona, Spain) and dehydrated in a graded series of ethanol after, before they were embedded in Paraplast®. Longitudinal microtome (Shandon Finesse 325) sections with 5 µm thickness were prepared throughout the defect site. The sections were stained with hematoxylin-erythrosin for new bone formation visualization. Bone mineralization was assessed with VOF trichrome staining. Red and brown staining indicates advanced mineralization, whereas less mineralized, newly formed bone stains in blue [19].

Sections were analyzed by light microscopy (LEICA DM 4000B) and computer based image

analysis software (Leica Q-win V3 Pro-image Analysis System, Barcelona, Spain) was used to evaluate all sections. A region of interest (ROI) within the defect (12.5 mm^2) was defined for quantitative evaluation of new bone formation. New bone formation was expressed as a percentage of repair with respect to the original defect area within the ROI. From the total bone repair, the areas of mature bone (MB) and immature bone (IB) were determined in the VOF staining sections, and the MB/IB ratio for each experimental group was calculated.

For immunohistochemical analysis, sections were deparaffined and rehydrated in Tris-buffered saline (TBS) (pH 7.4, 0.01 M Trizma base, 0.04 M Tris hydrochloride, 0.15 M NaCl), which was used for all further incubations and rinse steps. Sections were incubated in citrate buffer (pH 6) at 90ºC for antigen retrieval, followed by incubation in 3% hydrogen peroxide in TBS buffer for 20 min to inactivate endogenous peroxidase activity. After a rinse step, sections were blocked with 2% FBS in TBS–0.2% Triton X-100 (blocking buffer). The indirect immunohistochemical procedure was carried out by incubating the sections with osteocalcin (OCN) antiserum (1/100) (Millipore, Barcelona, Spain) in blocking buffer overnight at 4 ºC. Sections were rinsed three times, then incubated with biotin-SP-conjugated donkey anti-rabbit F(ab0) fragment (1/500) (Millipore, Barcelona, Spain) in blocking buffer for 1 h followed by incubation in peroxidase-conjugated streptavidin (1/500) (Millipore, Barcelona, Spain) for 1 h. Peroxidase activity was revealed in Tris–HCl buffer (0.05 M, pH 7.6) containing 0.005% of 3.3’ diaminobencidine (Sigma, Poole, UK) and 0.01% hydrogen peroxide. Reaction specificity was confirmed by replacing the specific antiserum with normal serum or by pre-adsorption of the specific antiserum with the corresponding antigen. OCN staining was evaluated using computer-based image analysis software (ImageJ, NIH, Bethesda, MD). OCN staining was measured by applying a fixed threshold to select for positive staining within the ROI. Positive pixel areas were divided

by the total surface size (mm^2) of the ROI. Values were normalized to those measured from blank scaffolds and are reported as relative staining intensities.

Neovascularization was quantified by determining blood vessel density and vessel surface area within the ROI. For this purpose, sections were immunolabeled with an anti-CD34 monoclonal antibody (1/50) (DAKO, Barcelona, Spain) in blocking buffer overnight at 4ºC. Sections were rinsed three times, then incubated with biotin-SP-conjugated donkey anti-rabbit F(ab0) fragment (1/500) (Millipore, Barcelona, Spain) in blocking buffer for 1 h, followed by incubation in peroxidase-conjugated streptavidin (1/500) (Millipore, Barcelona, Spain) for 1 h. Peroxidase activity was revealed in Tris–HCl buffer (0.05 M, pH 7.6) containing 0.005% of 3.3' diaminobencidine (Sigma, Poole, UK) and 0.01% hydrogen peroxide. Reaction specificity was confirmed by replacing the specific antiserum with normal serum. Blood vessel density was expressed in absolute values and vessel surface area in mm^2 based on the quantitative evaluation of the ROI.

2.8.3 Micro-CT studies

MicroCT studies were acquired with a Quantum FX imaging system (Perkin Elmer. 940 Winter St. Waltham, Massachusetts. EEUU). This piece of equipment is specifically designed for small lab animals. Acquisition parameters were: Field Of View 20 mm, acquisition time 4.5 minutes, X-ray energy 50 kV and 200 uA. Image reconstruction was based on Feldkamp´s method. These parameters define a 512x512x512 voxels image with 0,04mm pixel size and 0,000064mm3 voxel size.

Images were analyzed by Preclinical Imaging Platform staff at Vall d´Hebron Researching Institute using AMIDE software (Copyright (c) 2000-2012 Andreas Loening). Briefly, a fixed size Region of Interest (ROI) was made in the image, centered and adjusted to the bone defect

created. Then the volume of the total tissue was measured adjusting the minimum threshold of the selection to the soft tissue. No maximum threshold value was applied in order to include all the voxels of the bone tissue.

In a posterior step, a secondary ROI was created adjusting the threshold to the bone density and including all the voxels with a radiodensity value over this threshold. The threshold values were fixed in both threshold selections due to a previous microCT system calibration. ROI volumes and bone volume/total volume ratio were calculated. Finally, a histogram of each sample was made. For this purpose we created a macro in Slicer software ((http://www.slicer.org). Using the ROI that include soft and bone tissues voxels distributions were represented according to the density of each voxel that compounds the image.

2.9 Statistical analysis

The statistical analysis of the data was completed using GraphPad PRISM (7.0) software. The normal distribution of the data was checked by the Shapiro-Wilk test. For normally distributed data, Student´s *t*-test or one-way ANOVA were applied for differences between two groups or multiple comparisons, respectively. Tukey *post-hoc* test was applied for multiple comparisons. For non-normally distributed data, Mann-Whitney nonparametric analysis or Kruskal-Wallis test with Dunn´s multiple comparisons tests were applied. In all cases, p values <0.05 were considered as significant, represented by symbols described in the graphs. Data are presented as mean ± standard deviation.

3. Results and discussion

The development of organic-inorganic composite 3D scaffolds was driven through the freeze-drying technique. The organic part consisted of enzymatically crosslinked gelatin network, whereas two types of bioceramics were evaluated for the inorganic phase. Thus, the gradual

incorporation of HA and calcium sulfate into the polymeric hydrogel resulted in three levels of reinforcement and seven different types of formulations. Some of the composite scaffolds could be seen in Supplementary Figure S1. First, we characterized the main properties of all prototypes and then preselect only the best candidates for further *in vitro* and *in vivo* assessment (Figure 1a).

3.1 Swelling capacity and degradation profile

Regarding the water uptake process by dried scaffolds, all the formulations showed great ability to swell. Although the incorporation of fillers does not affect the kinetics of such a process (all the samples were swollen after 1 h), the swelling ratio decreased proportionally with the level of reinforcement (Figure 1b). These results are in accordance with those presented recently by others in which the swelling ratio of gelatin-HA cryogels decreased with the increase of HA concentration [20-22].

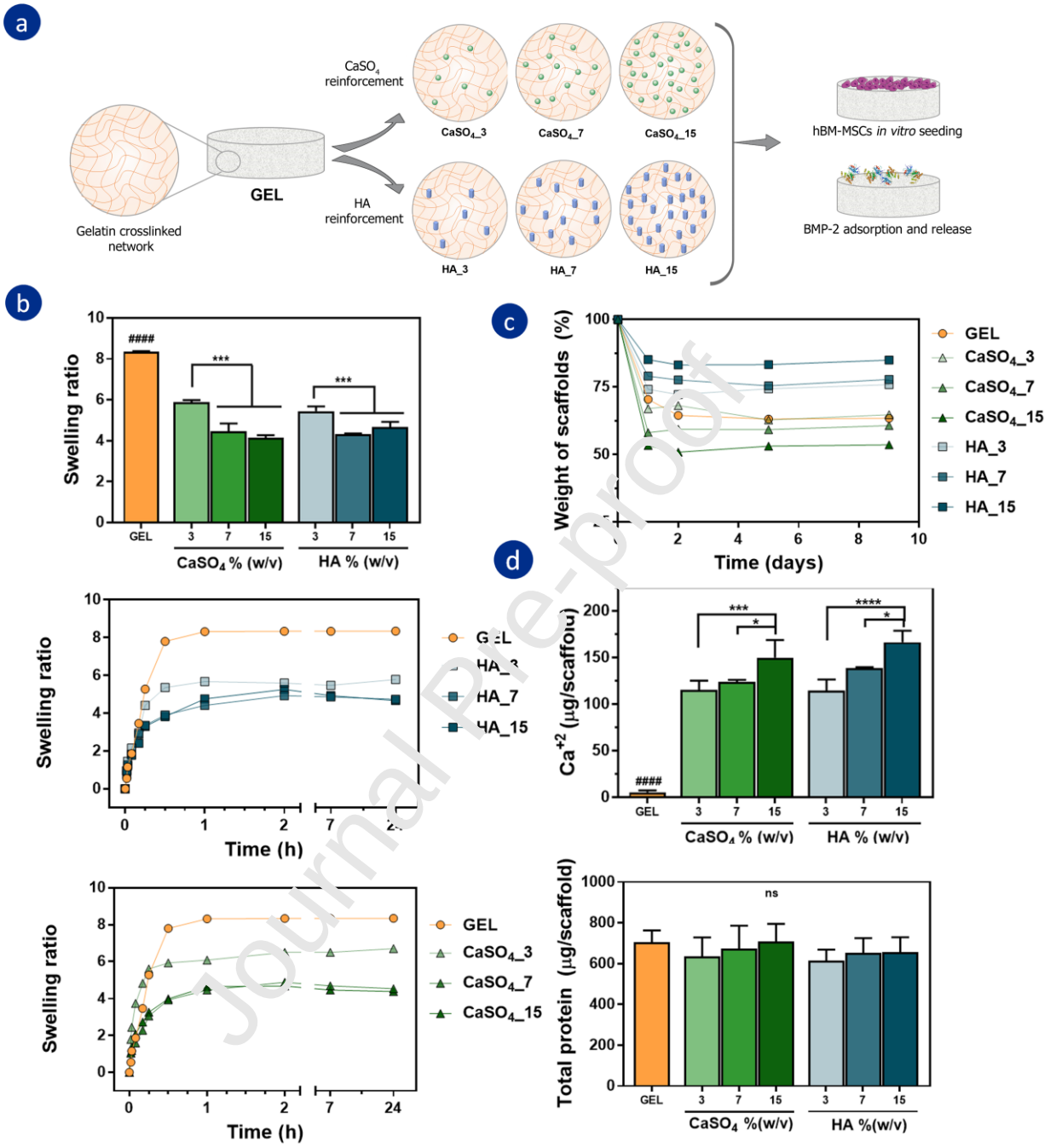

Figure 1. Development and characterization of reinforced gelatin-based scaffolds. (a) Schematic illustration of the design strategy of gradually reinforced gelatin scaffolds with either $CaSO_4$ or HA and the *in vitro* biological evaluation with hBM-MSCs seeding and BMP-2 growth factor delivery. (b) Determination of swelling properties of the systems. *In vitro* hydrolytic (c)

and enzymatic (d,e) degradation of the 3D scaffolds. Statistical significance: ns = no significant, * p<0.05, ** p<0.01, *** p<0.001 and **** p<0.0001; ### p<0.001 and #### p<0.0001 compared GEL to all the reinforced scaffolds.

Biodegradability is considered one of the most desirable features that a substitute designed for bone tissue regeneration must show [22,23]. In fact, a temporal structure that supports the neo-tissue growth but its degradation is coordinated with the regeneration process is still challenging for biomaterials designers. The analysis of the scaffold stability under hydrolytic conditions revealed a biphasic degradation profile for all the samples (Figure 1c). Because the calcium sulfate salt is more water-soluble than HA, the scaffolds reinforced with apatite ceramic showed lower hydrolytic degradation rate [24]. Although the study of the mechanism involved in this degradation is not within the scope of this work, we hypothesize that physical bulk erosion through the diffusion and dissolution of oligomers could be the responsible of the mass loss occurred during the first step [25]. Interestingly, the scaffolds remained stable for several days because the bonds that form the gelatin network were not hydrolytically cleaved. However, when the 3D matrices were immersed in the enzymatic solution that mimics better the *in vivo* environment, complete degradation of the samples was observed. Even so, the *in vitro* recapitulation of the surrounding conditions after the implantation of the scaffold is extremely challenging because of the presence of numerous families of proteases that control the extracellular matrix remodeling [26].

As expected, the calcium content accumulated because of the degradation of the scaffolds was proportional to the amount of inorganic bioceramic incorporated and the total amount of the proteins was the same for all the samples (Figure 1d). Interestingly, this release of calcium ions

as a consequence of the scaffold degradation could potentially promote a chemotactic paracrine effect to induce the recruitment of endogenous osteoprogenitor cells and to lead to their osteogenic differentiation. In fact, Aquino-Martinez R et al. have recently demonstrated similar bone regeneration with cell-free calcium containing scaffolds and scaffold seeded with MSCs in critical-sized calvarial defect model, suggesting the possibility to design cell-free and growth factor-free strategies for bone tissue engineering approaches [27].

3.2 Mechanical characterization

Uniaxial unconfined monotonic compression tests were performed to evaluate the Young modulus of the developed scaffolds (Figure 2a). The incorporation of inorganic components into gelatin-based organic network resulted in a significant increase in Young modulus from ~48 kPa to >75kPa, when compared to plain gelatin hydrogels (p<0.001). Interestingly, $CaSO_4$_15 scaffolds showed a 2-fold increase in Young modulus when compared to $CaSO_4$_3 scaffolds (209 ± 30 kPa versus 108 ± 9 kPa). Conversely, although the incorporation of HA resulted in a reinforcing effect compared to GEL scaffold, no statistically significant differences were observed between the different HA containing scaffolds. Some studies have demonstrated that hydrogels with a Young modulus similar to our HA-reinforced scaffolds (~ 60 kPa) induce optimal MSC osteogenesis both *in vitro* and *in vivo* [28]. However, the higher values of calcium sulfate-reinforced scaffolds may also be advantageous, particularly during the surgical insertion. In fact, although the bulk mechanical requirements for osteogenic 3D scaffolds designed to serve as resorbable temporary structures differ from those weight-bearing dense permanent implants, swollen 3D porous scaffolds must present enough stiffness to ensure proper surgical handling and stable graft fixation. In this regard, Zhang B. *et al.* have recently achieved exceptional results regarding the stable fixation rate, with multifunctional amphiphilic copolymer-HA composite

grafts presenting compressive modulus of 126-181 kPa after scaffolds hydration process [29].

Therefore, considering the preliminary examined physical and chemical properties, we limited the further characterization, biological commitment evaluation and *in vivo* bone regeneration performance assessment to scaffolds reinforced with 7.5% of calcium mineral elements and GEL scaffold as the control group.

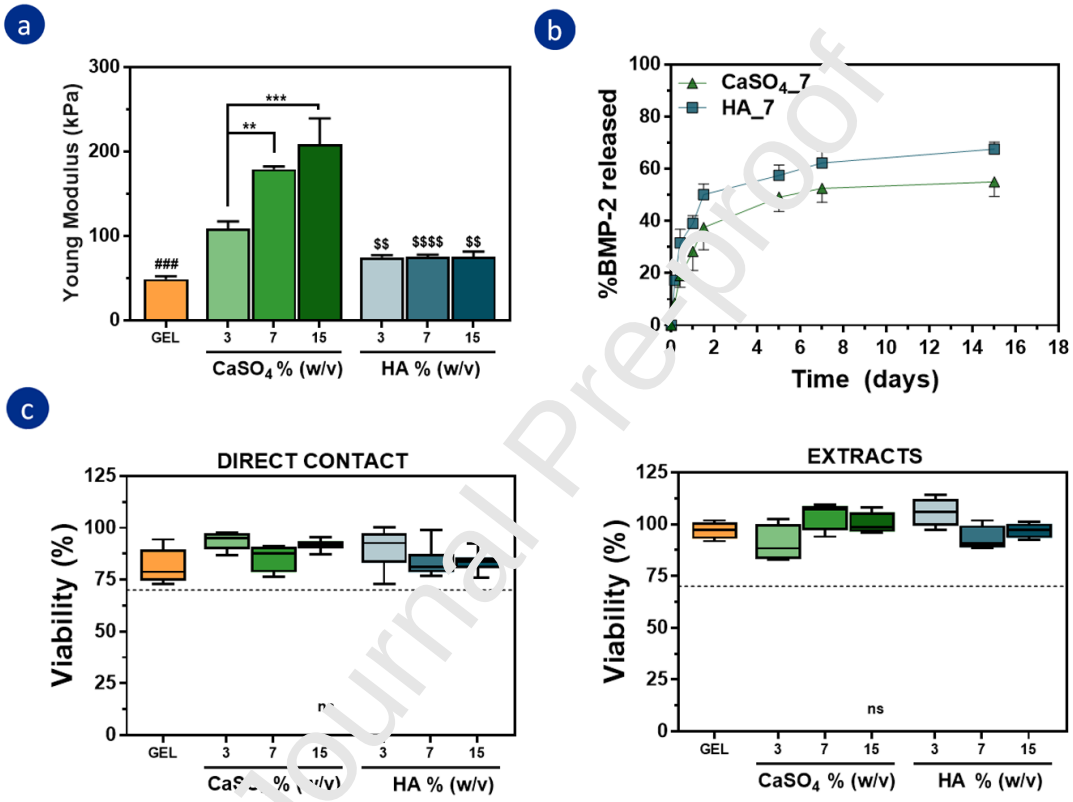

Figure 2. Further characterization studies of 3D organic-inorganic scaffolds. (a) Compressive mechanical properties of the developed material systems. (b) Biocompatibility properties assessed by extracts and direct contact cell-toxicity assays. (c) In vitro cumulative release of BMP-2 from the selected scaffolds. Statistical significance: ns = no significant, * p<0.05, ** p<0.01, *** p<0.001 and **** p<0.0001; ### p<0.001 and #### p<0.0001 compared

GEL to all the reinforced scaffolds.

3.3 Microstructure and elemental composition characterization

The microstructure analysis of the 3D scaffolds was performed by SEM. As shown in the representative SEM images depicted in Figure 3a, the scaffolds were porous. The pore size of the scaffolds is an important feature which influences the cell-cell interaction, cell migration, proliferation and differentiation processes during the regeneration of the tissue. In the case of the these scaffolds, the incorporation of ceramic compounds increased the size of pores, especially with HA inclusion. According to some previous studies, 3D scaffolds intended for bone tissue engineering with a pore size of around 100 µm may favor the migration and proliferation of osteoblast, thus promoting the bone formation [30]. Moreover, an efficient oxygen diffusion and waste and nutrient exchange between infiltrated cells the and the surrounding environment is expected with this range of pore size [31].

To properly examine the effective incorporation of osteoconductive minerals into the 3D gelatin structure, the evaluation of chemical structure was performed by means of EDAX mapping, FTIR and XRD analysis. Regarding EDAX measurements (Figure 3b), uniform distribution of calcium was noticed in both composite scaffolds. As expected, sulfur and phosphorous elements were observed in $CaSO_4$_7 and HA_7 composite scaffolds, respectively. The presence of reinforcing minerals was confirmed via the FTIR spectra. Infrared spectra of raw materials and the scaffolds are shown in Figure 3c. The characteristic bands of gelatin in 1023 (C-O-C stretching), 1342 (Amide III) and 3289 (Amine peak) cm^{-1} were observed in all the scaffolds. In the case of $CaSO_4$_7 scaffold, the amide I peak of gelatin shifted from 1634 to 1622 cm^{-1}. In addition, characteristic bands of the sulfate groups (SO_4^{-2}) were observed in this

composite scaffold: 1112 (ν_4 antisymmetric stretch vibration) and 596, 665 cm^{-1} (ν_4 antisymmetric bending vibration). On the other hand, regarding the spectra of scaffold reinforced with HA, the characteristic Amide II peak of gelatin shifted from 1535 to 1543 cm^{-1}. Moreover, the absorption bands at 601, 558 cm^{-1} (ν_4 bending vibration of phosphate groups) and 1029 cm^{-1} (ν_3 streching vibration of phosphate groups) confirmed the presence of HA within the composite scaffold. The functional incorporation of both reinforcing calcium minerals was further confirmed with XRD analysis (Figure 3d), since HA associated peaks (002), (211), (300) [32,33] and calcium sulfate corresponding peaks (110), (310), (220) and (-114) [34,35] were recorded in respective composites. Interestingly, the crystalline structure of HA and calcium sulfate remained the same after the composite formation.

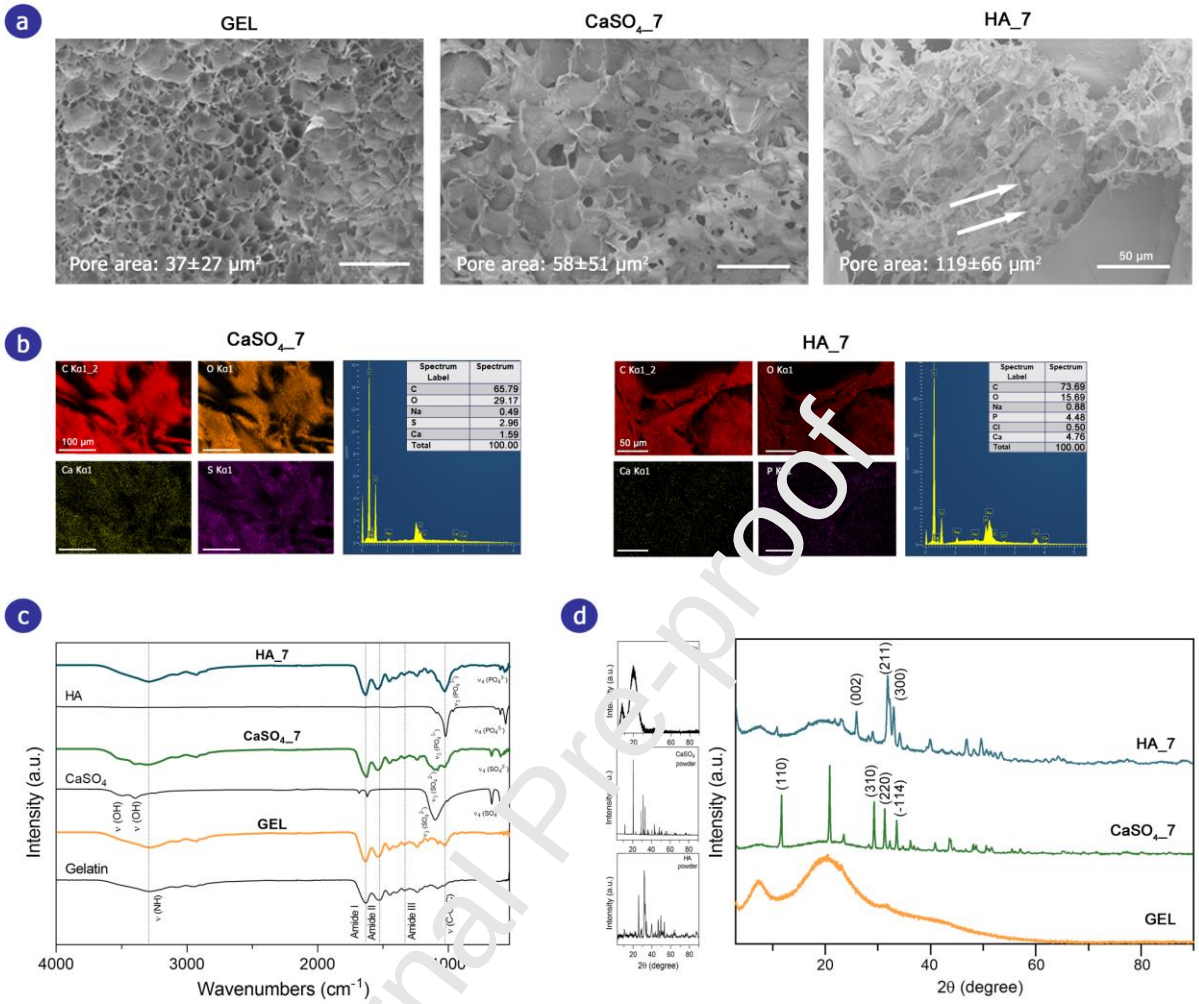

Figure 3. Morphological and chemical composition characterization of the gelatin-based composite scaffolds. (a) Representative SEM images of lyophilized scaffolds. White arrows point HA particles. (b) EDAX elementary mapping and the corresponding spectrum of the osteoconductive mineral composites. FTIR spectra (c) and XRD patterns (d) of pristine materials and developed gelatin-based composite scaffolds.

3.4 In vitro release of BMP-2

The release profile of bioactive BMP-2 factor from the organic/inorganic composite scaffolds (Figure 1b) demonstrated that the developed biomaterials facilitate the release of the osteogenic

growth factor over a period. The first burst release of the protein from the scaffolds was within the first 2 days and just 35-50% of the loaded BMP-2 was delivered in that period. Following that phase, the release of the growth factor was maintained from both gelatin scaffolds reinforced either with calcium sulfate or HA particles and around the 50 and 60% of the loaded dose was delivered until the end of the assay, respectively.

The spatiotemporal release of therapeutic factors at the injured site is a major challenge associated to the growth factors based therapies for tissue regeneration. Due to the short half-life of these biological factors, the use of supraphysiological doses to achieve the desired therapeutic effect is inevitably accompanied by several adverse effects that limit the consolidation and expansion of these therapies in the usual clinical practice [36]. For instance, ectopic bone formation, renal complications and cytotoxic effects have been broadly observed with the use of INFUSE® bone graft clinically approved for lumbar spinal fusion promotion [9]. Even though more advanced and complex systems with growth factors encapsulated in micro and nanoparticles as well as gene-therapy approaches [37,38] are being investigated to improve the spatiotemporal control of the therapeutic agents, it is expected that the bioactive constructs developed through the simple soak loading procedure may improve the strict regulatory concerns regarding the clinical translation [11]. Therefore, we hypothesize that enhancing the osteoconductive properties of the drug carrier by means of adding calcium components to the formulation could favor the reduction of the required dose of the BMP-2 for the therapeutic effect and relieve the side effects associated with high dosing levels.

Importantly, we have previously demonstrated that the scaffold GEL, suggested as a control in this experimental work, has the capacity to promote the sustained release of soak-loaded BMP-2 and the angiogenic factor VEGF following the first order kinetic. In that case, the burst release of

approximately 50% VEGF and 40% BMP-2 was evident within the first day [16]. Hence, the incorporation of reinforcing components does not affect the innate ability of the gelatin to guide the prolonged release of biological agents. Moreover, apart from the interactions between the positive charges of BMP-2 and negatively charged sites of gelatin [39,40], the slight extension of the burst effect notices over time could be probably because of non-specific electrostatic interactions occurred between the anionic groups of the sulfates and phosphate salts and the cationic groups of the growth factor [41,42].

3.5 Cell adhesion, proliferation and viability

The *in vitro* cytotoxic effect of implantable scaffolds was evaluated through indirect test with extracts and direct contact assay, using L929 fibroblasts as cell model. All experimental values exceeded the threshold limit established for non-cytotoxic biomaterials according to ISO10993 guidelines (Figure 2c). Therefore, unlike others calcium-phosphate based biomaterials [43], the range of bioceramics used in this work (3-15 % (w/v)) did not reveal any toxic effect on the cells due to the plausible ionic changes in the culture medium. Moreover, the ability of selected prototypes to support the cell adhesion and proliferation was evaluated with hBM-MSCs seeding on their surface. The use of these primary cells to assess the *in vitro* biological performance and to determine the osteoinductive properties of 3D scaffolds is broadly studied because of their easy accessibility, high osteogenic differentiation ability and the elevated replicative potential [44]. In addition, many efforts are being made to develop autologous bone grafts with cells isolated from the same patient [45,46]. Regarding the viability of cells seeded onto the surface of the scaffolds evaluated by a live/dead assay, high rates of viability were achieved in all the samples (Figure 4a). Above 80% of the cells were alive after 10 days of culture, and no significant differences between the groups were observed (Figure 4b). These anchorage-

dependent cells need to adhere to the surfaces to maintain their viability and osteogenic potential [47]. The fluorescent staining of the cytoskeleton and nuclei showed that the cells were completely adhered and spread on the surface of the scaffolds (Figure 4c). The mechanism beyond this adhesion may be mediated by the interaction between the integrin receptors present in cell membranes and the RGD motifs of the gelatin [48]. Furthermore, apart from the cellular adhesion produced on the surface of the scaffold, the cells proliferated during the *in vitro* culture as suggested by the increase in metabolic activity recorded between days 2 and 7 (Figure 4d). The cells could have reached confluence in a week, since the values of the CCK-8 assay did not increase from that moment [49]. However, no significant differences on proliferation rates among the scaffolds were detected throughout the entire period, suggesting that suitable platforms have been developed for osteoprogenitor cells to appropriately perform their role in the healing process.

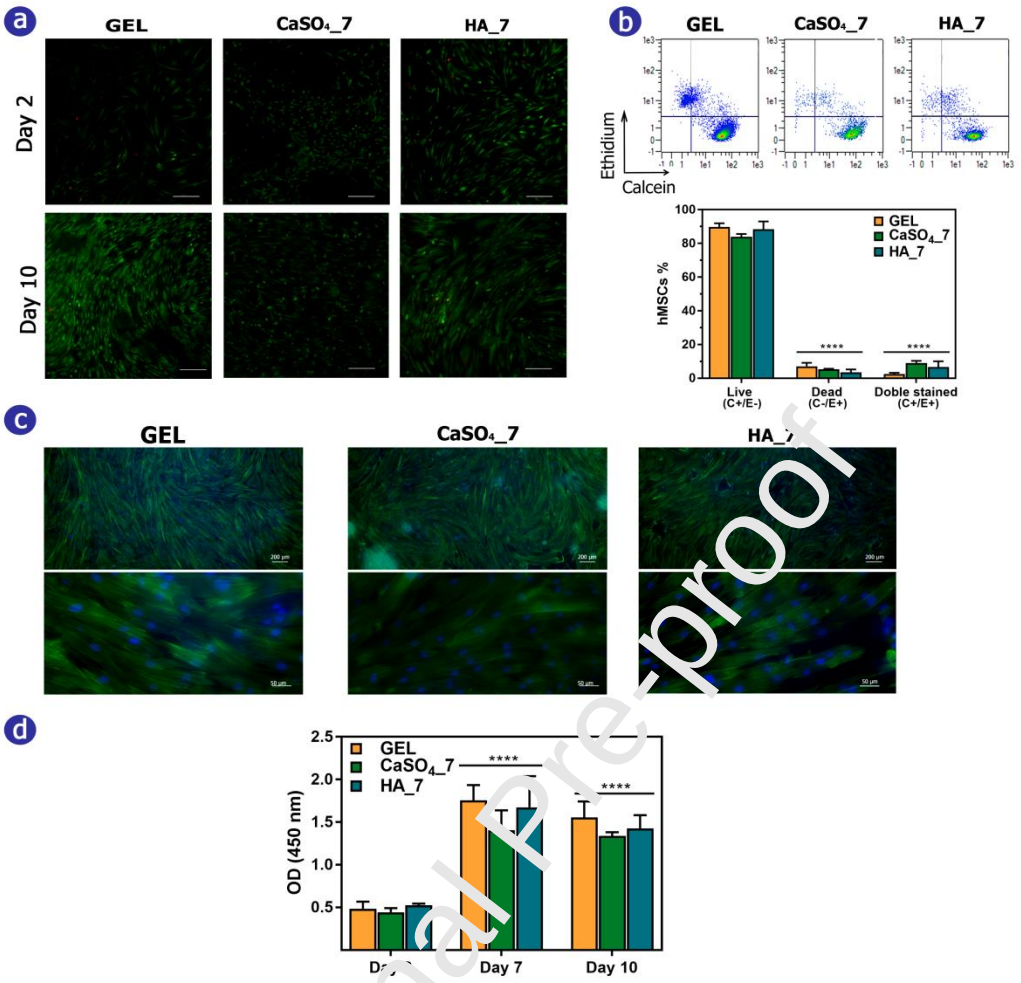

Figure 4. Adhesion, proliferation and viability of human bone-marrow derived mesenchymal stem cells (hBM-MSCs) seeded onto gelatin scaffolds. (a) Representative images of hBM-MSCs cultured onto the scaffolds for 2 and 10 days and Live/Dead staining. Scale bars = 500 µm (b) Quantification of cellular viability in different scaffolds after 10 days of culture analyzed by flow cytometry. (c) Fluorescence microscopy images of hBM-MSCs stained for nuclei (blue) and F-actin (green) after 7 days of culture on the scaffolds. (d) Metabolic activity of the cells cultured on the scaffolds for 2-10 days. Statistical differences: **** p<0.0001.

3.6 Assessment of osteogenic commitment

The evaluation of *in vitro* osteogenic differentiation potential of hBM-MSCs seeded on developed 3D scaffolds relied on the determination of ALP activity and the expression levels of

two stemness (*Nanog*, *Oct4*) and three osteogenic (*Col1a1*, *Runx2*, *Fmod*) marker genes. First, the secreted ALP activity of cells was quantified for 3 weeks (Figure 5a). The ALP activity of the cells seeded in the bare gelatin scaffold (GEL) remained constant throughout the culture period, while a constant increase was determined in the case of the organic/inorganic composite scaffolds. In addition, this increase was more noticeable for scaffolds formulated with HA. These differences were further contrasted with the qualitative chromogenic detection of this phosphatase at the end of the assay (Figure 5b). In the case of HA_7, the 50% of the scaffold surface was positively stained, while the covered area in the case of GEL was less than 10%. These results may suggest that the incorporation of the calcium elements to the gelatin scaffold could potentially enhance the osteconductive properties of the formulation and promote the osteogenic commitment of host stem cells during the healing process. In fact, the ALP is an early bone marker protein involved directly in the process of the biomineralization. ALP hydrolyzes the pyrophosphate to generate inorganic phosphate, which is deposited in the form of HA when the accumulation of calcium and phosphate ions exceeds their solubility [50].

In an attempt to better understand the cell differentiation process, an analysis of the expression level of several marker genes was performed. The results from the RT-PCR assay are shown in Figure 5c and the changes in genes expression suggested that cells seeded on the scaffolds were evolved through differentiation processes. For instance, the expression levels of stemness genes (*Nanog*, *Oct4*) were downregulated over the time for all the scaffolds. On the other hand, a dissimilar pattern was observed for genes related to osteogenic differentiation. While the expressions of *Col1a1* and *Fmod* were upregulated during the course of the culture, the expression of *Runx2* remained stable. In addition, these results were in accordance with the ALP determination assay, because the increase showed in the expression of some osteogenic marker

genes was more notable for scaffolds containing HA. Interestingly, the changes produced in the fate of the cells were caused only by the composition and structure of the scaffolds, since basal culture medium without any osteogenic supplementation was used for these experiments. In fact, external physical and chemical factors are considered to modulate the intracellular signaling pathways responsible for the orchestration of the differentiation of MSCs. Although the transcription factor *Runx2* is considered as the main regulator in osteogenic differentiation through several signaling pathways such as canonical and non-canonical BMP, Wnt/β-catenin or ERK1/2 signaling pathways[51,52], researchers still exploring other signaling routes and molecular mechanism involved in the regulation of the osteogenic differentiation [53,54]. For instance, some recent studies have concluded that the direct interaction between *Osterix* transcription factor and NFATc1 cofactor can promote the activation of the *Col1a1* gene promoter without activating the Runx2-dependent transcription [55,56]. Thus because of the effects of calcineurin-NFAT pathway has on the bone, potential therapeutic targets of this pathway are being considered for the development of new anabolic drugs for the treatment of osteoporosis. Recently Huang Y. et al demonstrated that the activation of this signaling pathway plays an important role in the anabolic effect of resveratrol on osteoblasts. For this reason, it seems necessary to extend the study of the cellular fate to conclude with more certainty the direction of the differentiation process and to describe the interactions between the hBM-MSCs and the developed scaffolds [57-59].

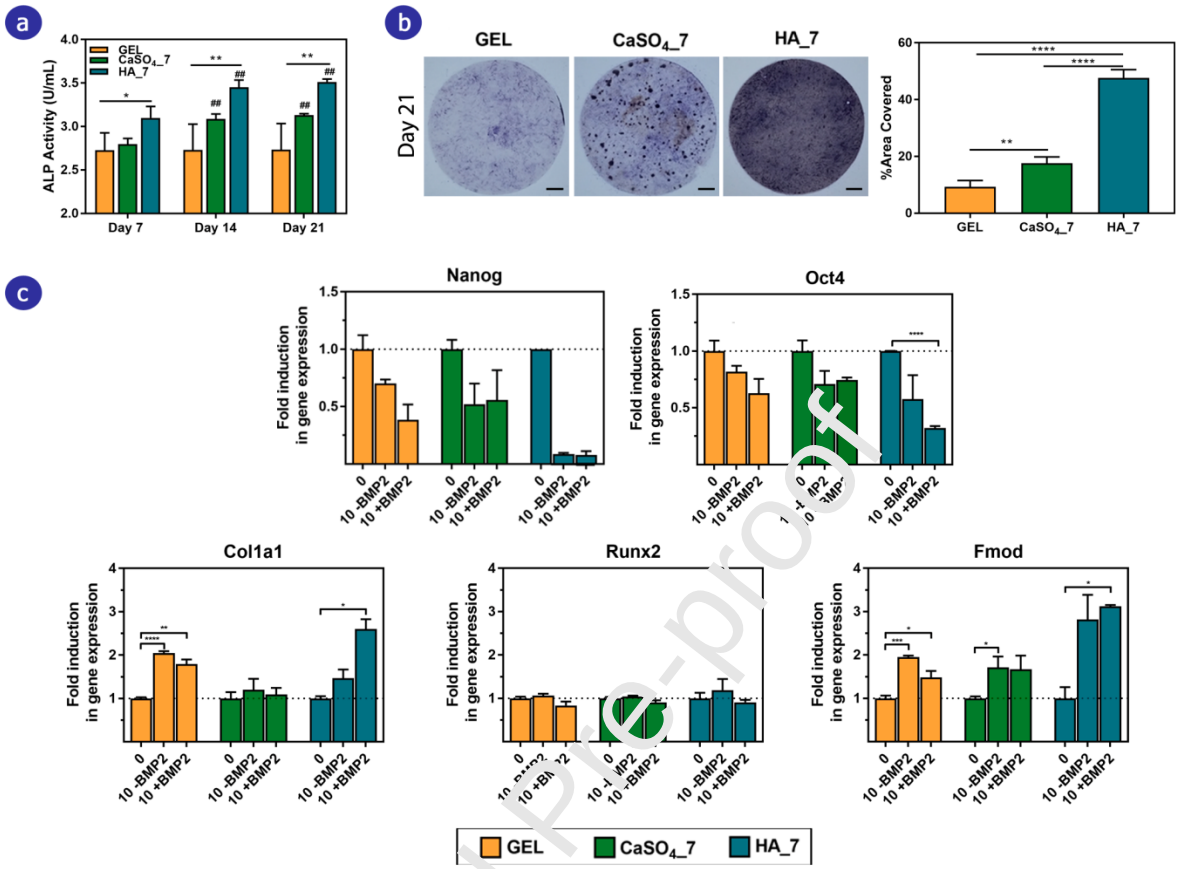

Figure 5. Evaluation of human bone marrow derived mesenchymal stem cells (hBM-MSCs) osteogenic commitment after cultured on the developed scaffolds. (a) Determination of alkaline phosphatase (ALP) activity secreted by hBM-MSCs after 7, 14 and 21 days of culture. (b) ALP staining images and the relative quantification of the stained area after 21 days of cell culture. Scale bars = 1.5 mm. (c) The expression level of five selected gene markers at 10 days after incubation. The expression levels of all genes were normalized to that of *Tbp* as the housekeeping gene. Statistical differences: * $p<0.05$, ** $p<0.01$, *** $p<0.001$ and **** $p<0.0001$; ## $p<0.01$ compared with the same scaffold at day 7.

3.7 Bone regeneration in osteoporotic mice bone defect

The potential of gelatin/bioceramic composite scaffold as osteogenic growth factor delivery carriers promoting bone healing was assessed in an osteoporotic mice calvaria defect model. The

model was carefully evaluated by histomorphometric parameters to confirm the experimentally induced osteoporotic state (Table S1 Supporting information).

The animals were divided into 5 experimental groups and the evaluation of the repair was performed 8 weeks after the induction of the critical-sized bone defect. The defects were empty in the control group and the developed 3D composite blank scaffolds or scaffolds loaded with BMP-2 were implanted in the rest of animals. Although many studies have been completed around the development of carriers for osteoinductive growth factors, most of these approaches have been evaluated in healthy animals defect models. However, disparate results have been achieved regarding the bone repair with same formulation loaded with BMP-2 in healthy and osteoporotic rats. These findings suggest the necessity to assess the bone regeneration potential of developed systems in specific animal models [60]. The combination of ovariectomy of female rodents and continuous administration of corticosteroids during 4 months has been previously validated as an osteoporosis model induction, showing altered structural characteristics of calvaria bone [61]. In fact, the healing process of flat bones such as calvaria, is negatively influenced by osteoporosis disease. The delay on bone repair associated with osteoporosis is further complicated in critical sized bone defects due to diminish self-healing ability of the diseased bones.

The histological images of the harvested defect areas revealed regenerated new bone tissue and bone microarchitecture in which developed 3D scaffolds were implanted (Figure 5a). Nevertheless, the repair response was limited in the control group (empty defect) and in the groups with blank scaffolds without growth factor loading. Nevertheless, in these experimental groups, the presence of newly formed bone was restricted to the margins of the defect and connective tissue that sometimes invaded the defect. In contrast, the functionalization of these

scaffolds with BMP-2 growth factor allowed the increase of the repair response in comparison with the control group and the blank scaffolds. In these cases, around the half of the defect surface was occupied by newly formed bone. However, a more compact structure was detected with the implantation of HA_BMP-2 scaffolds, and several regions revealed early mineralization of an extracellular matrix of connective-bone transition (Figure 6a, indicated with *). Promisingly, in these areas groups of osteocytes-like cells were also observed (Figure 6a, indicated with arrowheads).

The quantitative histomorphometric analysis corroborated these observation and the repair percentages of control, $CaSO_4$ and HA groups were 9, 12.8 and 14%, respectively. Although a trend of improvement was detected with the implantation of blank scaffolds, these differences were not statistically significant. Conversely, the inclusion of the therapeutic factor BMP-2 in the developed systems improved notoriously the regeneration capability. Thus, the repair response with HA_BMP-2 and $CaSO_4$_BMP-2 were 48.4% and 53.5% respectively, without significant differences between them (Figure 6b). Regarding the MB/IB ratio determination, groups treated with BMP-2 showed ratios of 1 in the $CaSO_4$ group and 1.15 in the HA group, showing values around 0.8 in the targets and the control group (Figure 6c).

Overall, although the results were not statistically significant, it can be concluded that fabricated gelatin/bioceramic scaffolds may possess osteoinductive and osteoconductive properties themselves. The histological analysis of the HA and $CaSO_4$ scaffolds without the growth factor showed formation of new bone in the margins of the defect occupying areas of certain importance, despite the fact that the repair percentages in these groups were low -slightly less than 15%-. This is a clear histological sign of osteoinductive and especially osteoconductive properties of biomaterials. In addition to this, the absence of inflammatory infiltrates and

histological signs of rejection of the material, indicates that they are biocompatible, which intensifies osteoinductive and osteoconductive properties to a certain extent. However, the incorporation of BMP-2 to the system is vital for a better osteogenic regeneration as it can be seen in the results. BMP-2, which is osteoinductive, enabled an improved bone formation.

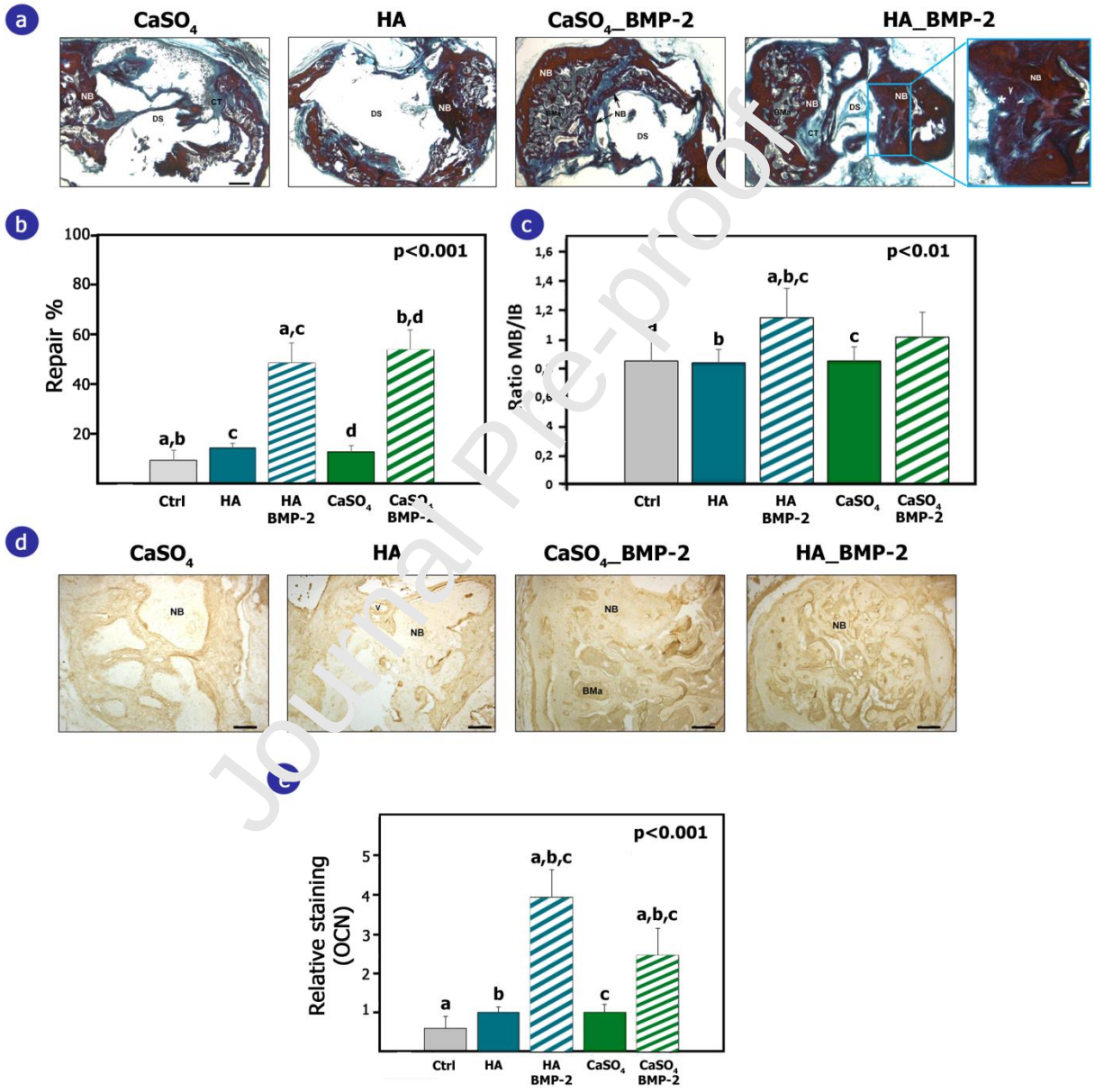

Figure 6. Bone regeneration assessment on osteoporotic mice calvaria defects 8 weeks after implantation of developed 3D scaffolds. (a) Representative VOF staining images in horizontal

section showing the defect site in the different experimental groups. The region marked with the blue box stands out in the HA-BMP group, which is shown at high magnification, shows an early mineralization zone defined as extracellular matrix of conjunctive-bone transition stained red (*) in which groups of osteocytes-like cells (arrowheads) are detected. Scale bars: Panoramic images = 500 µm. Detail image = 50 µm. (b) Quantitative analysis of histomorphometry showing the percentage of repair. (c) The ratio of mature bone (MB) and inmature bone (IB). (d) Representative images in horizontal section showing OCN immunoreactive staining in the defect site. Scale bar = 100 µm. (e) Relative OCN staining in arbitrary units in the different experimental groups. The same letters on different histograms indicates significant differences between these groups. BMa: Bone marrow, CT: Connective tissue, DS: Defect site, NB: Newly formed bone, v: Blood vessel.

To further explore the neotissue observed in the defect site 8 weeks after the 3D scaffolds implantation, osteocalcin (OCN), a late marker of osteogenesis and mineralization, expression was analyzed (Figure 6d). The immunohistochemistry images revealed higher relative expression level of OCN in composite scaffolds loaded with BMP-2 groups in comparison to the control and blank scaffolds groups (Figure 6e). These results were in accordance with histological and histomorphometric data, suggesting the suitability of developed organic/inorganic composite scaffolds as osteogenic drug delivery carriers. Unlike those observed in the repair response from histological analysis, the OCN expression was significantly higher in HA_BMP-2 group compared to $CaSO_4$ scaffolds loaded with osteoinductive growth factor. On the other hand, vascularization analysis at the defect site revealed the presence of higher density and vascular surface area in the experimental groups treated with BMP-2 in relation to the blank groups and

the control group (Figure 7). Uniform distribution of the neovascularization was shown in all the experimental groups.

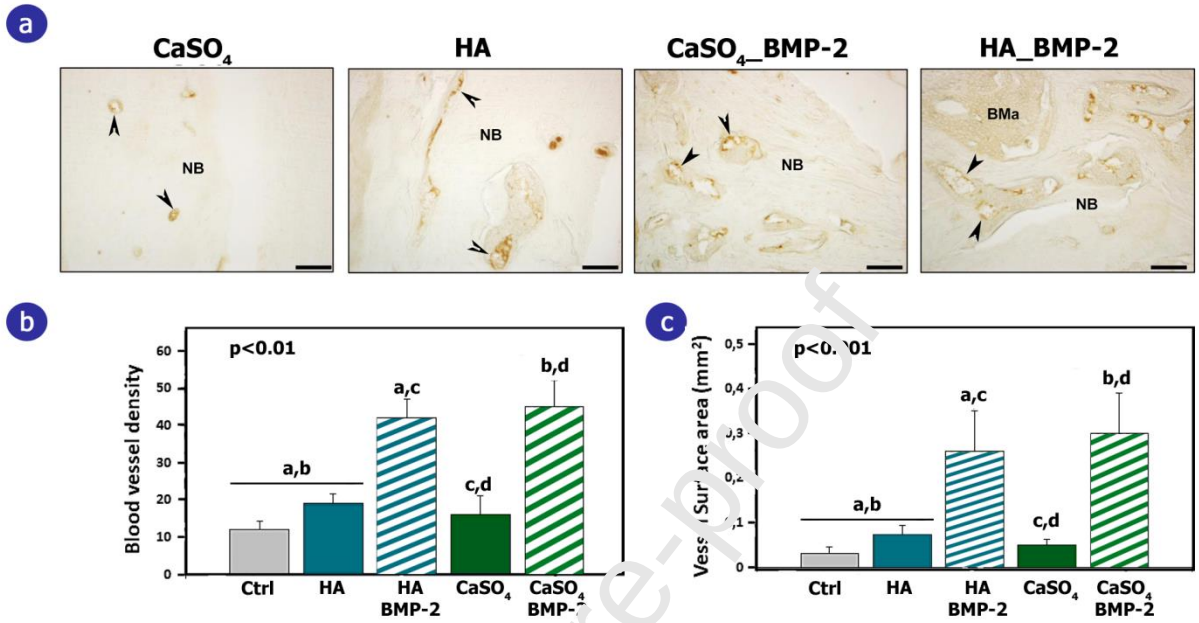

Figure 7. Analysis of the vascularization of newly formed tissue on the defect site. (a) Representative images in horizontal section showing CD34 immunoreactive staining in the defect site in the different experimental groups 8 weeks post-implantation. The immunoreaction can be seen in the endothelial cells lining the lumen of the blood vessels (arrowheads). The blood vessel density (b) and vessel surface area (c) within the ROI in the different experimental groups. The same letters on different histograms indicates significant differences between these groups. BMa: Bone marrow, NB: Newly formed bone. Scale bar = 70 µm.

In order to macroscopically confirm the results of the histological and histomorphometric analysis of the effect of BMP-2 on the regeneration process, a micro-CT analysis was performed in the groups treated with this growth factor. The analysis revealed in both groups repair percentages referred to as BV/TV (bone volume / total defect volume), identical, in the CaSO4 BMP-2 group (53.9%), and somewhat higher in the HA BMP-2 group (66.2%), with respect to

those obtained in the histomorphometric analysis. The micro-CT images and videos reveal, in both groups, large areas of radiopaque material compatible with areas of bone repair at the margins of the lesion (Figure S2, Supporting information). In the HA BMP-2 group, discrete areas of radiopaque material are also observed inside the defect that could correspond to areas of bone repair, however the percentages obtained in this group differ slightly upwards from those obtained by histomorphometry, which could be explained based on the presence of HA in the scaffold, which is detected as radiopaque material not distinguishable from the surrounding bone tissue, and can be counted as repaired area when in fact they are not.

4. Conclusions

In this study, we have successfully engineered bioinspired organic/inorganic composite 3D scaffolds, integrating calcium sulfate and HA bioceramics into the enzymatically crosslinked gelatin network. The reinforced systems showed higher pore size, increased compressive mechanical properties and good biocompatibility profile. In addition, hBM-MSCs exhibited efficient adhesion and proliferative capacities on the organic/inorganic composite scaffolds and osteogenic differentiation patterns were recorded in systems prepared with both bioceramics. The optimization of the experimental conditions and the potential proteomic analysis could elucidate the in vivo biological impact produced by the 3D scaffolds after their implantation on the host osteoprogenitor cells. These reinforced scaffolds were capable of promoting in vitro sustained release of BMP-2 after loading the therapeutic factor though soak-loading procedure, without the need of complex delivery systems. Interestingly, the osteoconductive gelatin/bioceramics composite functionalized with BMP-2 promoted bone regeneration in osteoporotic mice calvarial defect. Overall, the developed gelatin-based composites may be useful as scaffolds for bone regeneration in osteoporotic defects, avoiding supraphysiological doses and reducing

consequently the possible adverse effects.

ASSOCIATED CONTENT

Micro-CT images and quantification; animal model histomorphometric analisis (PDF)

Animations showing alternately the regenerated area in dorsal and ventral view (MPG)

Author Contributions

The manuscript was written through contributions of all authors. All authors have given approval to the final version of the manuscript.

ACKNOWLEDGMENT

Orive G wish to thank the Spanish Ministry of Economy, Industry, and Competitiveness (PID2019-106094RB-I00/AEI/10.13039/501100011033) and technical assistance from the ICTS NANBIOSIS (Drug Formulation Unit, U10) at the University of the Basque Country. We also appreciate the support from the Basque Country Government (Grupos Consolidados, No ref: IT907-16). Echave MC and Erezuma I thanks to the Basque Government for the PhD grant (PRE_2020_2_0042).

REFERENCES

[1] J.A. Kanis, L.J. Melton, C. Christiansen, C.C. Johnston, N. Khaltaev, The diagnosis of osteoporosis, J. Bone Miner. Res. 9 (1994) 1137-1141.

[2] O. Johnell, J.A. Kanis, An estimate of the worldwide prevalence and disability associated with osteoporotic fractures, Osteoporos. Int. 17 (2006) 1726-1733.

[3] S. Muruganandan, H.J. Dranse, J.L. Rourke, N.M. McMullen, C.J. Sinal, Chemerin neutralization blocks hematopoietic stem cell osteoclastogenesis, Stem cells . 31 (2013) 2172-2182.

[4] L. Liao, X. Yang, X. Su, C. Hu, X. Zhu, N. Yang, X. Chen, S. Shi, Y. Jin, Redundant miR-3077-5p and miR-705 mediate the shift of mesenchymal stem cell lineage commitment to adipocyte in osteoporosis bone marrow, Cell Death Dis. 4 (2013) e600.

[5] A. Decambron, A. Fournet, M. Bensidhoum, M. Manassero, F. Sailhan, H. Petite, D. Logeart-Avramoglou, V. Viateau, Low-dose BMP-2 and MSC dual delivery onto coral scaffold for critical-size bone defect regeneration in sheep, J. Orthop. Res. 35 (2017) 2637-2645.

[6] I.H.A. Ali, D.P. Brazil, Bone morphogenetic proteins and their antagonists: current and emerging clinical uses, Br. J. Pharmacol. 171 (2014) 3620-3632.

[7] G. Muzio, G. Martinasso, F. Baino, R. Frairia, C. Vitale-Brovarone, R.A. Canuto, Key role of the expression of bone morphogenetic proteins in increasing the osteogenic activity of osteoblast-like cells exposed to shock waves and seeded on bioactive glass-ceramic scaffolds for bone tissue engineering, J Biomater Appl. . 29 (2014) 728-736.

[8] S. Kargozar, S.J. Hashemian, M. Soleimani, P.B. Milan, M. Askari, V. Khalaj, A. Samadikuchaksaraie, S. Hamzehlou, A.R. Katebi, N. Latifi, M. Mozafari, F. Baino, Acceleration of bone regeneration in bioactive glass/gelatin composite scaffolds seeded with bone marrow-derived mesenchymal stem cells over-expressing bone morphogenetic protein-7, Mater. Sci. Eng. C. 75 (2017) 688-698.

[9] E.J. Carragee MD, Hurwitz, Eric L., DC, PhD, D.K. Weiner MD, A critical review of recombinant human bone morphogenetic protein-2 trials in spinal surgery: emerging safety concerns and lessons learned, Spine J. 11 (2011) 471-491.

[10] W. McKay, S. Peckham, J. Badura, A comprehensive clinical review of recombinant human bone morphogenetic protein-2 (INFUSE® Bone Graft), Int. Orthop. 31 (2007) 729-734.

[11] D.P. Walsh, R.M. Raftery, G. Chen, A. Heise, F.J. O'Brien, S. Cryan, Rapid healing of a critical- sized bone defect using a collagen- hydroxyapatite scaffold to facilitate low dose, combinatorial growth factor delivery, J. Tissue Eng. Regen. Med. 13 (2019) 1843-1853.

[12] J. Ran, P. Jiang, S. Liu, G. Sun, P. Yan, X. Shen, H. Tong, Constructing multi-component organic/inorganic composite bacterial cellulose-gelatin/hydroxyapatite double-network scaffold platform for stem cell-mediated bone tissue engineering, Mater. Sci. Eng. C. Mater. Biol. Appl. 78 (2017) 130-140.

[13] T. Miyazaki, A. Sugawara-Narutaki, C. Ohtsuki, Organic-Inorganic Composites Toward Biomaterial Application, Biomaterials for Oral and Craniomaxillofacial Applications, S. Karger AG, Basel, Switzerland, 2015, pp. 33-38.

[14] M.C. Echave, R. Hernáez-Moya, L. Iturriaga, J.L. Pedraz, R. Lakshminarayanan, A. Dolatshahi-Pirouz, N. Taebnia, G. Orive, Recent advances in gelatin-based therapeutics, Expert Opin. Biol. Ther. 19 (2019) 773-779.

[15] V. Acosta Santamaría, J. García Aznar, I. Ochoa, M. Doblare, Effect of Sample Pre-Contact on the Experimental Evaluation of Cartilage Mechanical Properties, Exp. Mech. 53 (2013) 911-

917.

[16] M.C. Echave, C. Pimenta-Lopes, J.L. Pedraz, M. Mehrali, A. Dolatshahi-Pirouz, F. Ventura, G. Orive, Enzymatic crosslinked gelatin 3D scaffolds for bone tissue engineering, Int. J. Pharm. 562 (2019) 151-161.

[17] M. Rodríguez-Évora, A. Delgado, R. Reyes, A. Hernández-Daranas, I. Soriano, J. San Román, C. Évora, Osteogenic effect of local, long versus short term BMP-2 delivery from a novel SPU–PLGA–βTCP concentric system in a critical size defect in rats, Eur. J. Pharm. Sci. 49 (2013) 873-884.

[18] A. Hernández, R. Reyes, E. Sánchez, M. Rodríguez-Évora, A. Delgado, C. Évora, In vivo osteogenic response to different ratios of BMP-2 and VEGF released from a biodegradable porous system, J. Biomed. Mater. Res. A. 100A (2012) 2382-2391.

[19] E. Martínez-Sanz, D.A. Ossipov, J. Hilborn, S. Larsson, K.B. Jonsson, O.P. Varghese, Bone reservoir: Injectable hyaluronic acid hydrogel for minimal invasive bone augmentation, J. Control. Release. 152 (2011) 232-240.

[20] L. Gu, J. Zhang, L. Li, Z. Du, Q. Cai, X. Yang, Hydroxyapatite nanowire composited gelatin cryogel with improved mechanical properties and cell migration for bone regeneration, Biomed. Mater. 14 (2019) 045001.

[21] N. Kemence, N. Bolgen, Gelatin- and hydroxyapatite- based cryogels for bone tissue engineering: synthesis, characterization, in vitro and in vivo biocompatibility, J. Tissue Eng. Regen. Med. 11 (2017) 20-33.

[22] Y. Zhang, M. Chen, J. Tian, P. Gu, H. Cao, X. Fan, W. Zhang, In situ bone regeneration enabled by a biodegradable hybrid double-network hydrogel, Biomater. Sci. 7 (2019) 3266-3276.

[23] G. Chen, W. Tang, X. Wang, X. Zhao, C. Chen, Z. Zhu, Applications of Hydrogels with Special Physical Properties in Biomedicine, Polymers. 11 (2019) 1420.

[24] H.H. Kim, J.B. Park, M.J. Kang, Y.H. Park, Surface-modified silk hydrogel containing hydroxyapatite nanoparticle with hyaluronic acid–dopamine conjugate, Int. J. Biol. Macromol. 70 (2014) 516-522.

[25] C. Engineer, J. Parikh, A. Raval, Review on hydrolytic degradation behavior of biodegradable polymers from controlled drug delivery system, Trends Biomater. Artif. Organs. 25 (2011) 79.

[26] C. Bonnans, J. Chou, Z. Werb, Remodelling the extracellular matrix in development and

disease, Nat. Rev. Mol. Cell Biol. 15 (2014) 786-801.

[27] R. Aquino-Martínez, D.G. Monroe, F. Ventura, Calcium mimics the chemotactic effect of conditioned media and is an effective inducer of bone regeneration, PloS one. 14 (2019) e0210301.

[28] N. Huebsch, E. Lippens, K. Lee, M. Mehta, S.T. Koshy, M.C. Darnell, R.M. Desai, C.M. Madl, M. Xu, X. Zhao, O. Chaudhuri, C. Verbeke, W.S. Kim, K. Alim, A. Mammoto, D.E. Ingber, G.N. Duda, D.J. Mooney, Matrix elasticity of void-forming hydrogels controls transplanted-stem-cell-mediated bone formation, Nat. Mater. 14 (2015) 1269-1277.

[29] B. Zhang, J.D. Skelly, J.R. Maalouf, D.C. Ayers, J. Song, Multifunctional scaffolds for facile implantation, spontaneous fixation, and accelerated long bone regeneration in rodents, Sci. Transl. Med. 11 (2019) eaau7411.

[30] I. Bružauskaitė, D. Bironaitė, E. Bagdonas, E. Bernotienė, Scaffolds and cells for tissue regeneration: different scaffold pore sizes—different cell effects, Cytotechnology. 68 (2016) 355-369.

[31] N. Annabi, J.W. Nichol, X. Zhong, C. Ji, S. Koshy, A. Khademhosseini, F. Dehghani, Controlling the porosity and microarchitecture of hydrogels for tissue engineering, Tissue Eng. Part B. Rev. 16 (2010) 371-383.

[32] M. Hasany, A. Thakur, N. Taebnia, F.B. Kadumudi, M. Shahbazi, M.K. Pierchala, S. Mohanty, G. Orive, T.L. Andresen, C.B. Foldager, S. Yaghmaei, A. Arpanaei, A.K. Gaharwar, M. Mehrali, A. Dolatshahi-Pirouz, Combinatorial Screening of Nanoclay-Reinforced Hydrogels: A Glimpse of the "Holy Grail" in Orthopedic Stem Cell Therapy? ACS Appl. Mater. Interfaces. 10 (2018) 34924-34941.

[33] T. Wu , B. Li, W. Wang, L. Chen, Z. Li, M. Wang, Z. Zha, Z. Lin, H. Xia, T. Zhang, Strontium-substituted hydroxyapatite grown on graphene oxide nanosheet-reinforced chitosan scaffold to promote bone regeneration, Biomater. Sci. 8 (2020) 463-4615.

[34] Q. Miao, S. Yang, H. Ding, J. Liu, Controlled degradation of chitosan-coated strontium-doped calcium sulfate hemihydrate composite cement promotes bone defect repair in osteoporosis rats, Biomed. Mater. (Bristol). 15 (2020) 55039-055039.

[35] R. Xu, X. Lian, Y. Shen, Y. Zhang, B. Niu, S. Zhang, Q. Guo, Q. Zhang, J. Du, F. Li, Q. Lu, D. Huang, Y. Wei, Calcium sulfate bone cements with nanoscaled silk fibroin as inducer, J. Biomed. Mater. Res. 107 (2019) 2611-2619.

[36] E. Nyberg, C. Holmes, T. Witham, W. Grayson, Growth factor-eluting technologies for bone tissue engineering, Drug Deliv. Transl. Res. 6 (2016) 184-194.

[37] T.D. Castillo Santaella, I. Ortega-Oller, M. Padial-Molina, O Valle Ravassa, Francisco Javier, P.A. Galindo Moreno, A.B. Jódar Reyes, J.M. Peula-García, Formulation, Colloidal Characterization, and In Vitro Biological Effect of BMP-2 Loaded PLGA Nanoparticles for Bone Regeneration, Pharmaceutics. 11 (2019) 388.

[38] R.M. Raftery, D.P. Walsh, I.M. Castaño, A. Heise, G.P. Duffy, S. Cryan, F.J. O'Brien, Delivering Nucleic-Acid Based Nanomedicines on Biomaterial Scaffolds for Orthopedic Tissue Repair: Challenges, Progress and Future Perspectives, Adv. Mater. 28 (2016) 5447-5469.

[39] J. Amirian, N.T.B. Linh, Y.K. Min, B. Lee, The effect of BMP-2 and VEGF loading of gelatin-pectin-BCP scaffolds to enhance osteoblast proliferation, J. Appl. Polym. Sci. 132 (2015) n/a.

[40] M. Yamamoto, Y. Takahashi, Y. Tabata, Controlled release by biodegradable hydrogels enhances the ectopic bone formation of bone morphogenetic protein, Biomaterials. 24 (2003) 4375-4383.

[41] X. Dong, Q. Wang, T. Wu, H. Pan, Understanding Adsorption-Desorption Dynamics of BMP-2 on Hydroxyapatite (001) Surface, Biophys. J. 93 (2007) 750-759.

[42] K. Wang, C. Zhou, Y. Hong, X. Zhang, A review of protein adsorption on bioceramics, Interface focus. 2 (2012) 259-277.

[43] A. Przekora, J. Czechowska, D. Pijocha, A. Ślósarczyk, G. Ginalska, Do novel cement-type biomaterials reveal ion reactivity that affects cell viability in vitro? Cent. Eur. J. Bio. 9 (2014) 277-289.

[44] H. Liu, D. Li, Y. Zhang, M. Li, Inflammation, mesenchymal stem cells and bone regeneration, Histochem. Cell Biol. 149 (2018) 393-404.

[45] M.W. Joo, S.J. Chung, S.H. Shin, Y. Chung, The effect of autologous platelet-rich plasma on bone regeneration by autologous mesenchymal stem cells loaded onto allogeneic cancellous bone granules, Cells Tissues Organs. 203 (2017) 327-338.

[46] A. Trounson, C. McDonald, Stem Cell Therapies in Clinical Trials: Progress and Challenges, Cell. Stem Cell. 17 (2015) 11-22.

[47] S. Lu, E. Lee, J. Lam, Y. Tabata, A. Mikos, Evaluation of Gelatin Microparticles as Adherent-Substrates for Mesenchymal Stem Cells in a Hydrogel Composite, Ann. Biomed. Eng.

44 (2016) 1894-1907.

[48] N. Davidenko, C. Schuster, D. Bax, R. Farndale, S. Hamaia, S. Best, R. Cameron, Evaluation of cell binding to collagen and gelatin: a study of the effect of 2D and 3D architecture and surface chemistry, J. Mater. Sci. Mater. Med. 27 (2016) 1-14.

[49] W. Chang, Z. Yang, T. Chong, Y. Liu, H. Pan, C. Lin, Quantifying Cell Confluency by Plasmonic Nanodot Arrays to Achieve Cultivating Consistency, ACS Sens. 4 (2019) 1816-1824.

[50] H. Orimo, The Mechanism of Mineralization and the Role of Alkaline Phosphatase in Health and Disease, J. Nippon Med. Sch. 77 (2010) 4-12.

[51] A. Zolocinska, The expression of marker genes during the differentiation of mesenchymal stromal cells, Adv. Clin. Exp. Med. 27 (2018) 717-723.

[52] L. Hu, C. Yin, F. Zhao, A. Ali, J. Ma, A. Qian, Mesenchymal Stem Cells: Cell Fate Decision to Osteoblast or Adipocyte and Application in Osteoporosis Treatment, Int. J. Mol. Sci. 19 (2018) 360.

[53] X. Wang, D. Zhao, Y. Zhu, Y. Dong, Y. Liu, Long non-coding RNA GAS5 promotes osteogenic differentiation of bone marrow mesenchymal stem cells by regulating the miR-135a-5p/FOXO1 pathway, Mol. Cell. Endocrinol. 496 (2019) 110534.

[54] T. Zhou, Y. Yan, C. Zhao, Y. Xu, Q. Wang, N. Xu, Resveratrol improves osteogenic differentiation of senescent bone mesenchymal stem cells through inhibiting endogenous reactive oxygen species production via AMPK activation, Redox Rep. 24 (2019) 62-69.

[55] N. Artigas, C. Ureña, E. Rodríguez-Carballo, J.L. Rosa, F. Ventura, Mitogen-activated Protein Kinase (MAPK)-regulated Interactions between Osterix and Runx2 Are Critical for the Transcriptional Osteogenic Program, J. Biol. Chem. 289 (2014) 27105-27117.

[56] H. Takayanagi, T. Koga, Y. Matsui, M. Asagiri, T. Kodama, B. de Crombrugghe, K. Nakashima, NFAT and Osterix cooperatively regulate bone formation, Nat. Med. 11 (2005) 880-885.

[57] S. Lu, Y. Hsia, K. Shih, T. Chou, Fucoidan Prevents RANKL-Stimulated Osteoclastogenesis and LPS-Induced Inflammatory Bone Loss via Regulation of Akt/GSK3β/PTEN/NFATc1 Signaling Pathway and Calcineurin Activity, Mar. Drugs. 17 (2019) 345.

[58] P.H. Stern, The Calcineurin-NFAT Pathway and Bone: Intriguing New Findings, Mol. Interv. 6 (2006) 193-196.

[59] Y. Huang, J. Huo, F. Liu, J. Liu, X. Zhang, C. Guo, L. Song, Resveratrol Promotes in vitro Differentiation of Osteoblastic MC3T3-E1 Cells via Potentiation of the Calcineurin/NFATc1 Signaling Pathway, Biochemistry Moscow. 84 (2019) 686-692.

[60] J.H. Lee, H. Baek, K. Lee, G.B. Zheng, S.J. Shin, H. Shim, Effects of ovariectomy and corticosteroid induced osteoporosis on the osteoinductivity of rhBMP-2 in a segmental long-bone defect model, Tissue Eng. Part A. 21 (2015) 2262-2271.

[61] E. Segredo-Morales, R. Reyes, M. Arnau, A. Delgado, C. Évora, In situ gel-forming system for dual BMP-2 and 17β-estradiol controlled release for bone regeneration in osteoporotic rats, Drug Deliv. Transl. Res. 8 (2018) 1103-1113.

Declaration of competing interests

☒ The authors declare that they have no known competing financial interests or personal relationships that could have appeared to influence the work reported in this paper.

☐The authors declare the following financial interests/personal relationships which may be considered as potential competing interests:

CRediT author statement

Echave MC: Conceptualization, Investigation, Formal analysis, Writing - Original Draft, Visualization
Erezuma I: Writing - Original Draft, Writing - Review & Editing
Golafshan N: Investigation
Castilho M: Review & Editing
Babu Kadumudi F: Investigation
Pimenta-Lopes C: Investigation
Ventura F: Investigation
Pujol A: Formal analysis
Jimenez JJ: Formal analysis
Camara J: Investigation
Hernáez-Moya R: Investigation
Iturriaga L: Investigation
Sáenz Del Burgo L: Review & Editing
Lloro I: Investigation, Review & Editing
Azkargorta M: Investigation, Review & Editing
Elortza F: Investigation, Review & Editing
Lakshminarayanan R: Review & Editing
Taleb H Al-Tel: Review & Editing
García-García P: Investigation
Reyes R: Investigation
Delgado A: Investigation
Évora C: Investigation
Pedraz JL: Conceptualization, Supervision, Project administration
Dolatshahi-Pirouz A: Conceptualization, Supervision, Project administration
Orive G: Conceptualization, Supervision, Project administration

Highlights:

- Gelatin/Bioceramic composite scaffolds were successfully created via freeze-drying.
- 3D scaffolds showed enhanced mechanical properties.
- Reinforced systems displayed better osteogenic properties in vitro.
- Bioceramic scaffolds were able to release BMP-2 in a sustained manner.
- Scaffolds embedded with supraphysiological doses of BMP-2 boost bone regeneration in vivo.

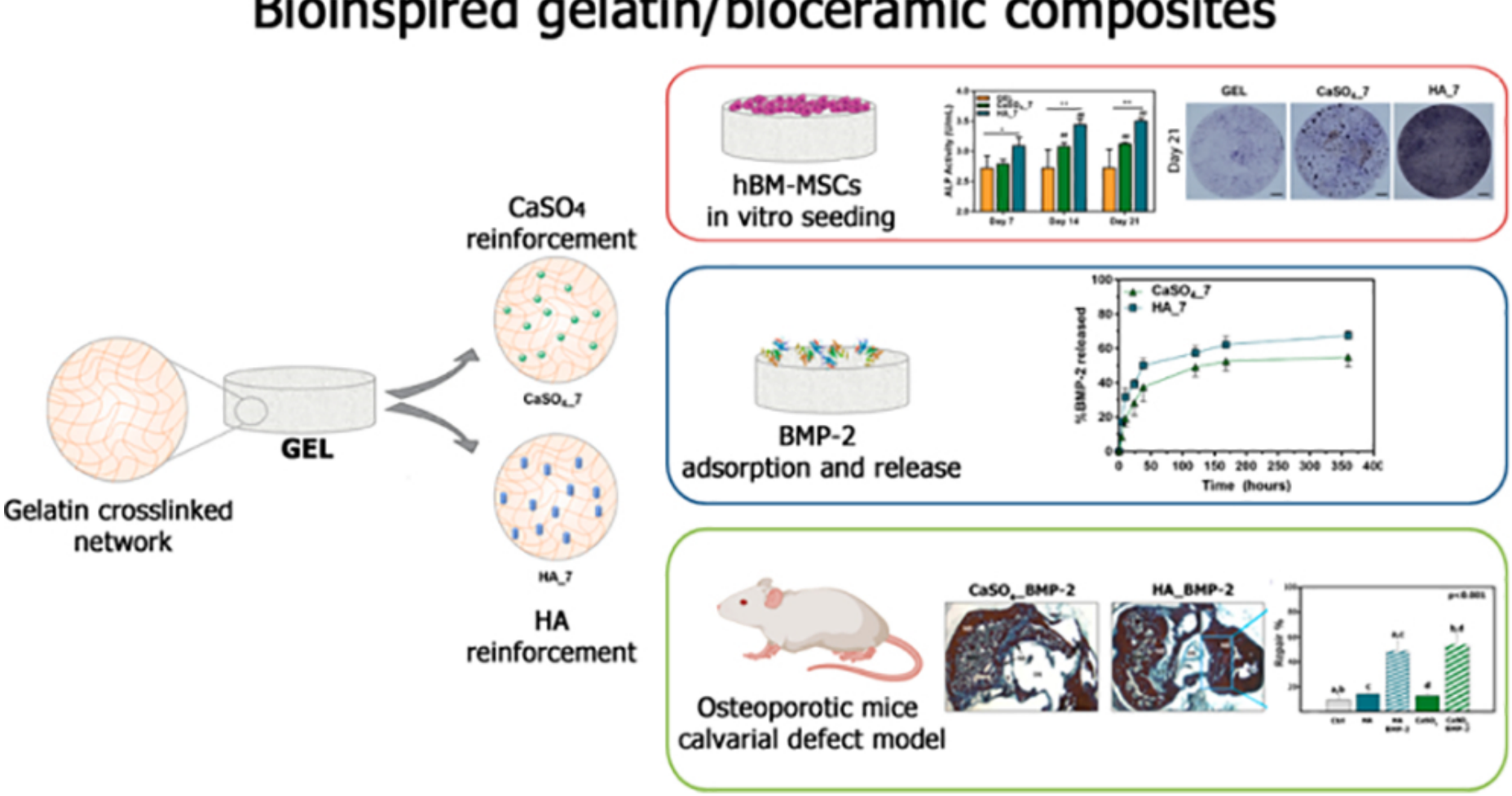

Graphics Abstract

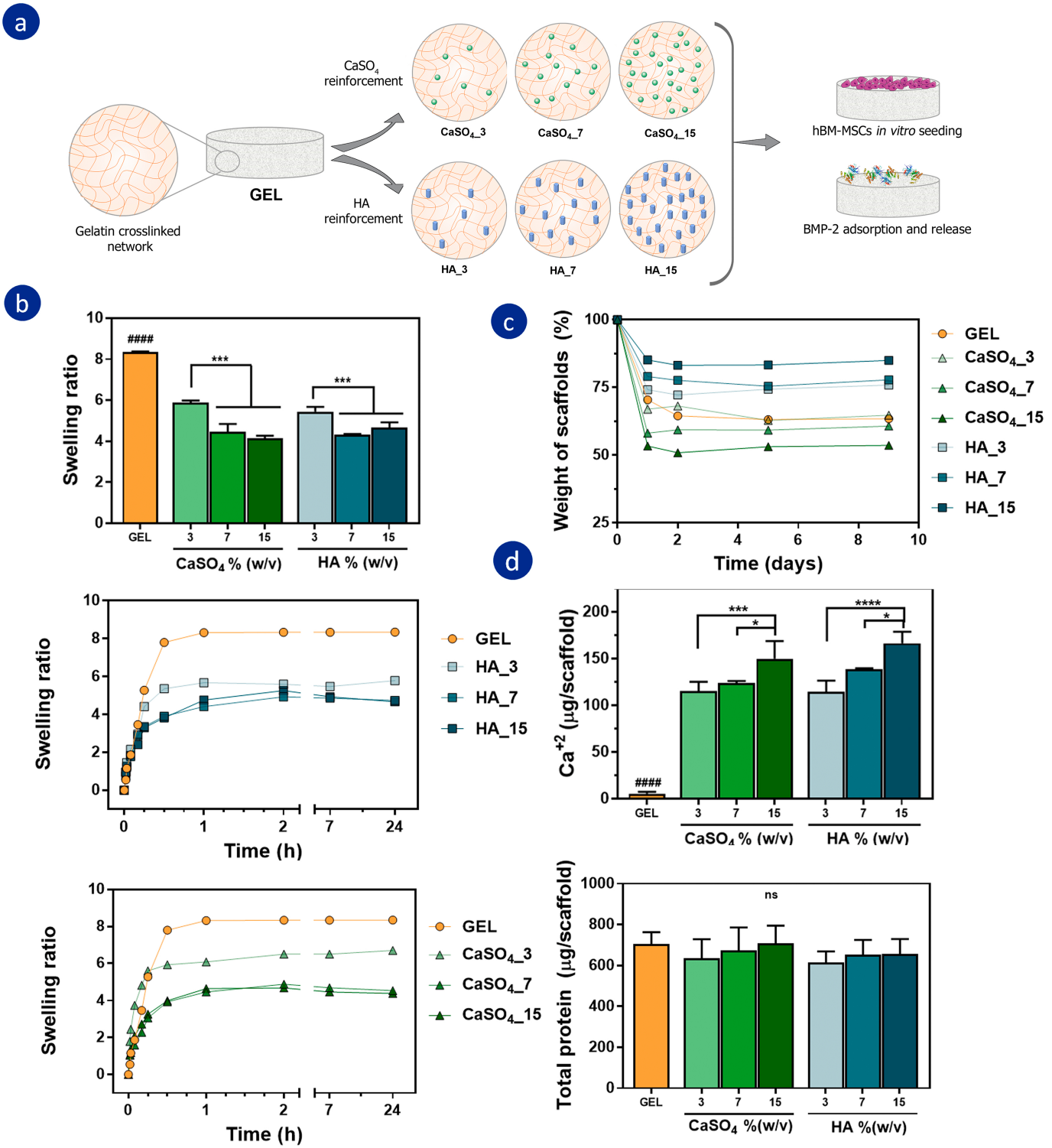
a
CaSO4 reinforcement
HA reinforcement
GEL
Gelatin crosslinked network
CaSO4_3
CaSO4_7
CaSO4_15
HA_3
HA_7
HA_15
hBM-MSCs in vitro seeding
BMP-2 adsorption and release
b
Swelling ratio
####
***
***
GEL
3
7
15
3
7
15
CaSO4 % (w/v)
HA % (w/v)
c
Weight of scaffolds (%)
Time (days)
GEL
CaSO4_3
CaSO4_7
CaSO4_15
HA_3
HA_7
HA_15
d
Swelling ratio
Time (h)
GEL
HA_3
HA_7
HA_15
Swelling ratio
Time (h)
GEL
CaSO4_3
CaSO4_7
CaSO4_15
Ca+2 (µg/scaffold)
***
*
****
*
####
GEL
CaSO4 % (w/v)
HA % (w/v)
Total protein (µg/scaffold)
ns
GEL
CaSO4 %(w/v)
HA %(w/v)

Figure 1

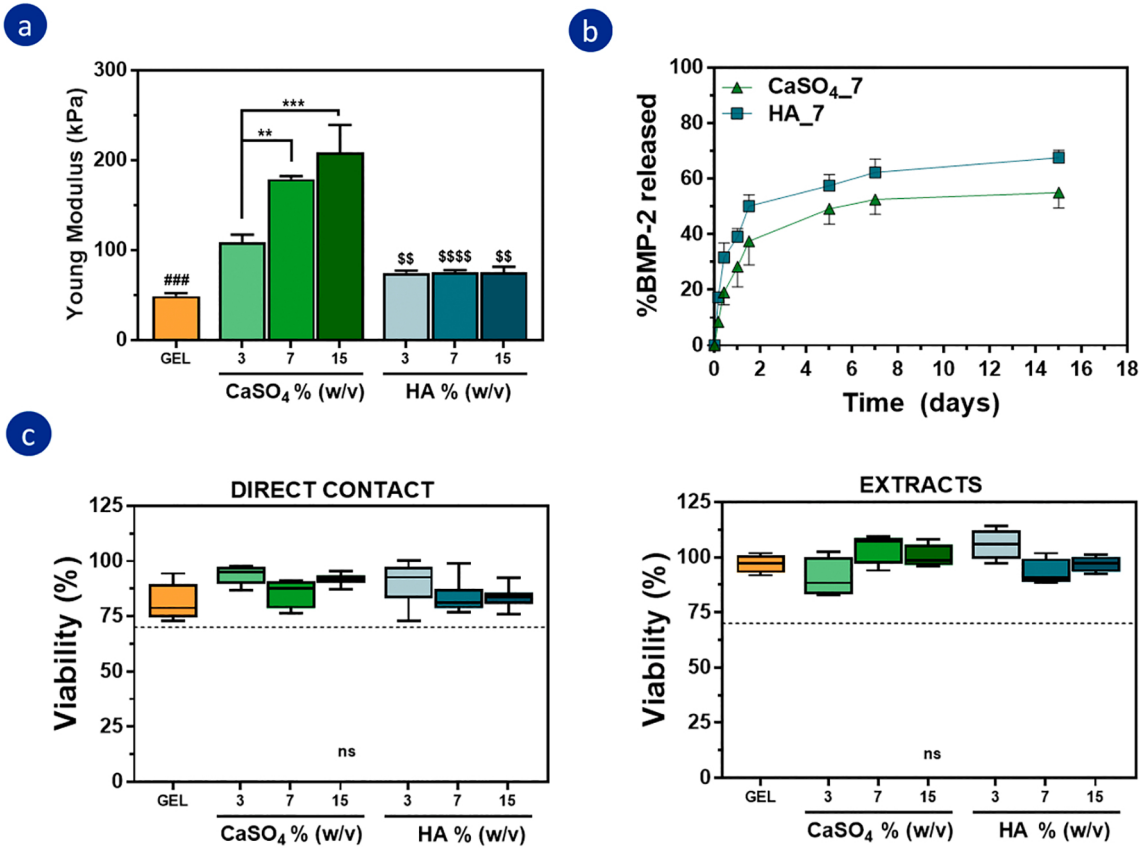
a
Young Modulus (kPa)
300
200
100
0
***
**
###
$$
$$$$
$$
GEL
3
7
15
3
7
15
CaSO4 % (w/v)
HA % (w/v)
b
%BMP-2 released
100
80
60
40
20
0
CaSO4_7
HA_7
0
2
4
6
8
10
12
14
16
18
Time (days)
c
DIRECT CONTACT
Viability (%)
125
100
75
50
25
0
ns
GEL
3
7
15
3
7
15
CaSO4 % (w/v)
HA % (w/v)
EXTRACTS
Viability (%)
125
100
75
50
25
0
ns
GEL
3
7
15
3
7
15
CaSO4 % (w/v)
HA % (w/v)

Figure 2

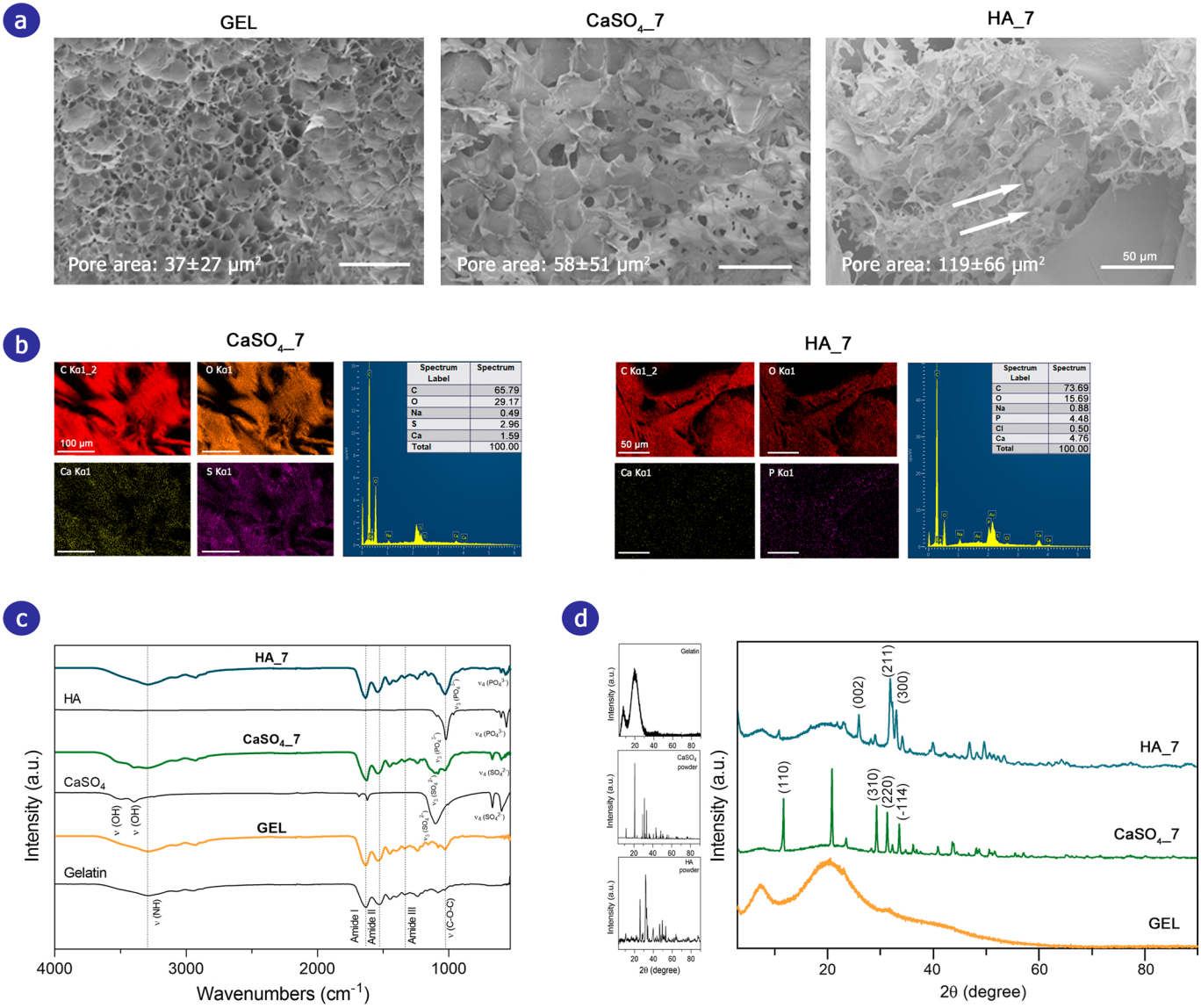
a
GEL
CaSO4_7
HA_7
Pore area: 37±27 µm²
Pore area: 58±51 µm²
Pore area: 119±66 µm²
50 µm
b
CaSO4_7
HA_7
C Kα1_2
O Kα1
Ca Kα1
S Kα1
P Kα1
100 µm
50 µm
Spectrum Label
Spectrum
C 65.79
O 29.17
Na 0.49
S 2.96
Ca 1.59
Total 100.00
C 73.69
O 15.69
Na 0.88
P 4.48
Cl 0.50
Ca 4.76
Total 100.00
c
HA_7
HA
CaSO4_7
CaSO4
GEL
Gelatin
Intensity (a.u.)
Wavenumbers (cm-1)
4000
3000
2000
1000
ν (OH)
ν (NH)
Amide I
Amide II
Amide III
ν (C-O-C)
d
Gelatin
CaSO4 powder
HA powder
2θ (degree)
(002)
(211)
(300)
(110)
(310)
(220)
(-114)
HA_7
CaSO4_7
GEL

Figure 3

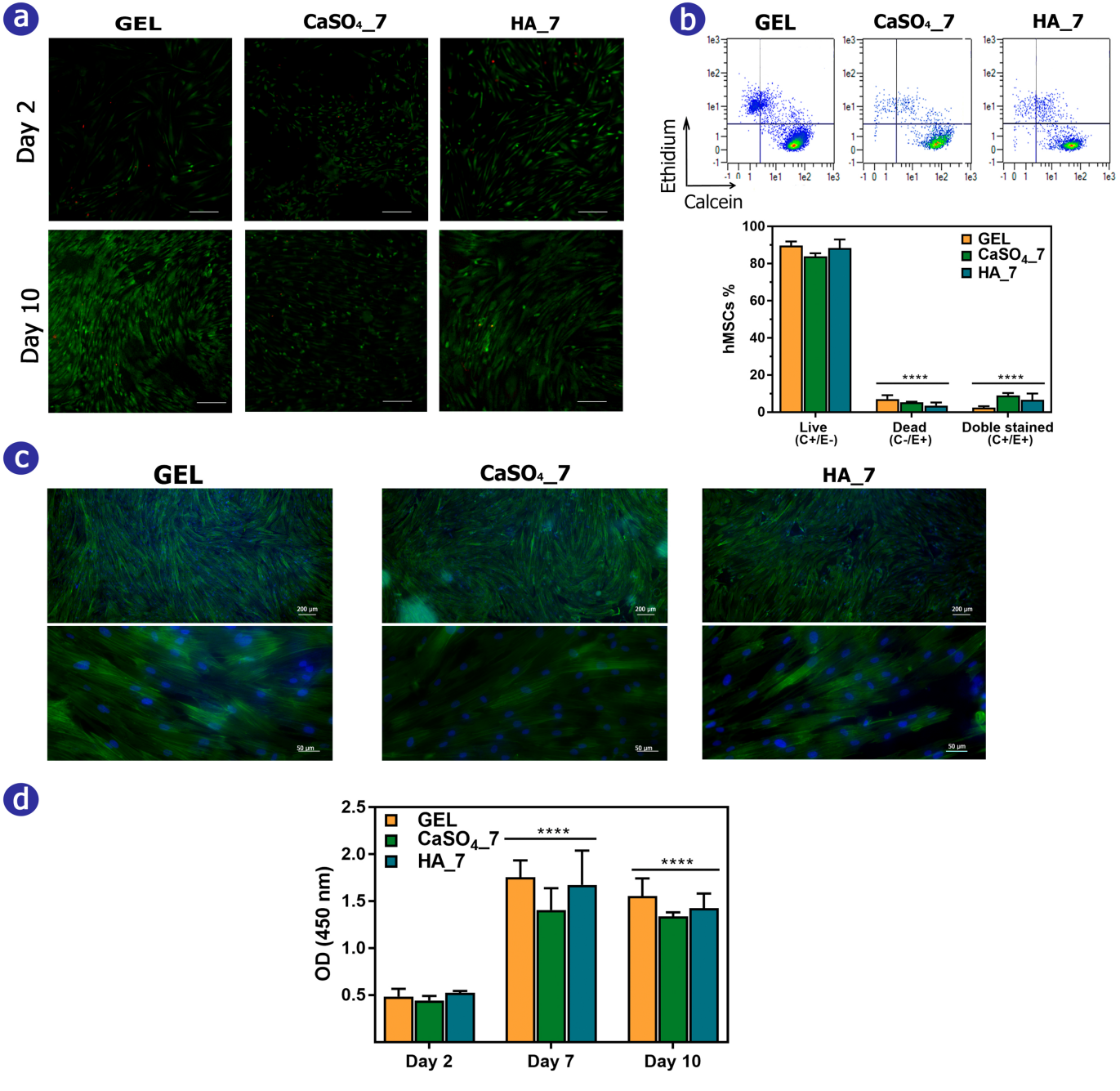
a
GEL
CaSO4_7
HA_7
Day 2
Day 10
b
GEL
CaSO4_7
HA_7
Ethidium
Calcein
hMSCs %
GEL
CaSO4_7
HA_7
****
****
Live
(C+/E-)
Dead
(C-/E+)
Doble stained
(C+/E+)
c
GEL
CaSO4_7
HA_7
200 µm
50 µm
d
OD (450 nm)
GEL
CaSO4_7
HA_7
****
****
Day 2
Day 7
Day 10

Figure 4

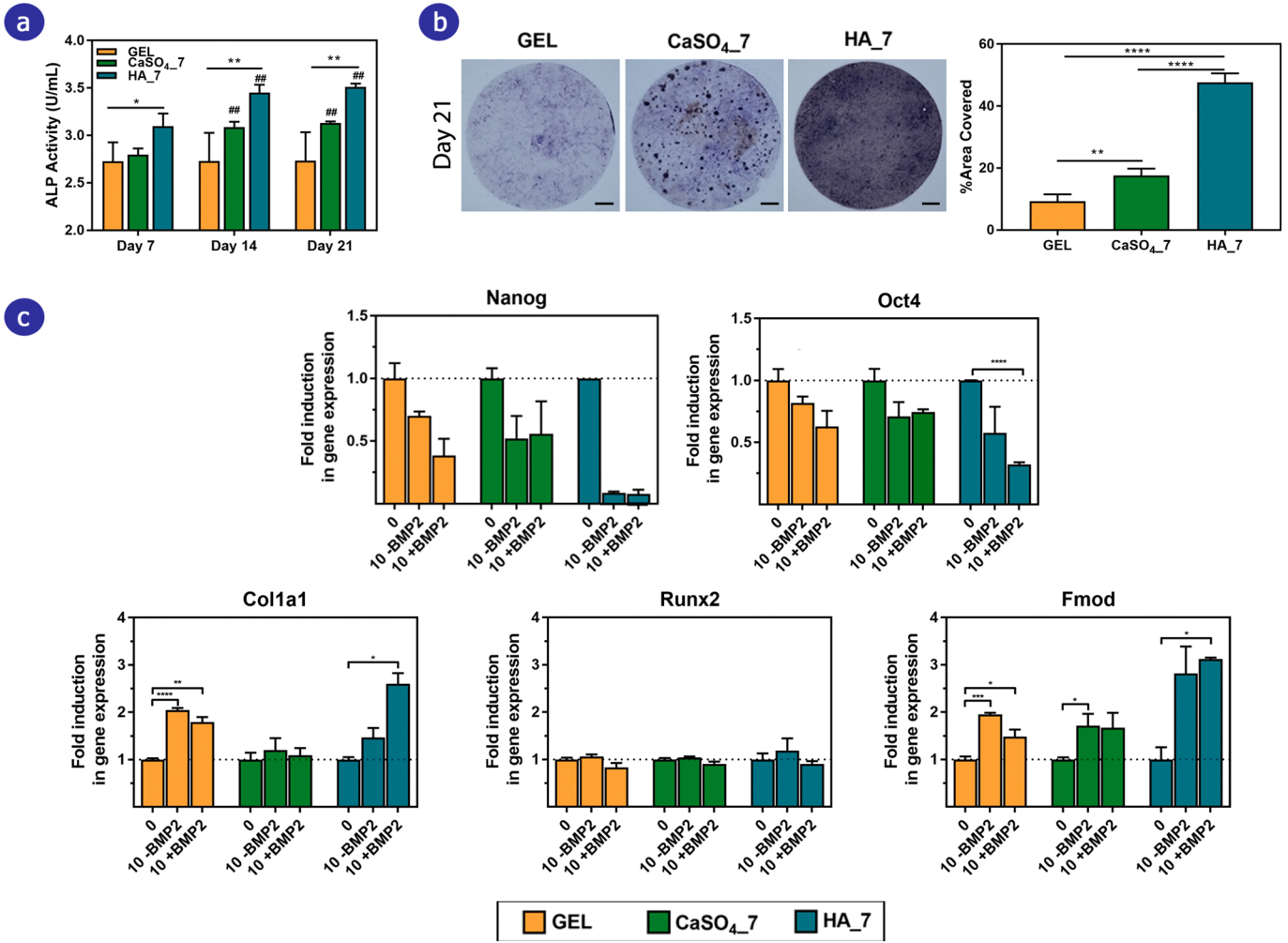
a
ALP Activity (U/mL)
GEL
CaSO4_7
HA_7
Day 7
Day 14
Day 21
b
GEL
CaSO4_7
HA_7
Day 21
%Area Covered
c
Nanog
Oct4
Col1a1
Runx2
Fmod
Fold induction in gene expression
0
10 -BMP2
10 +BMP2

Figure 5

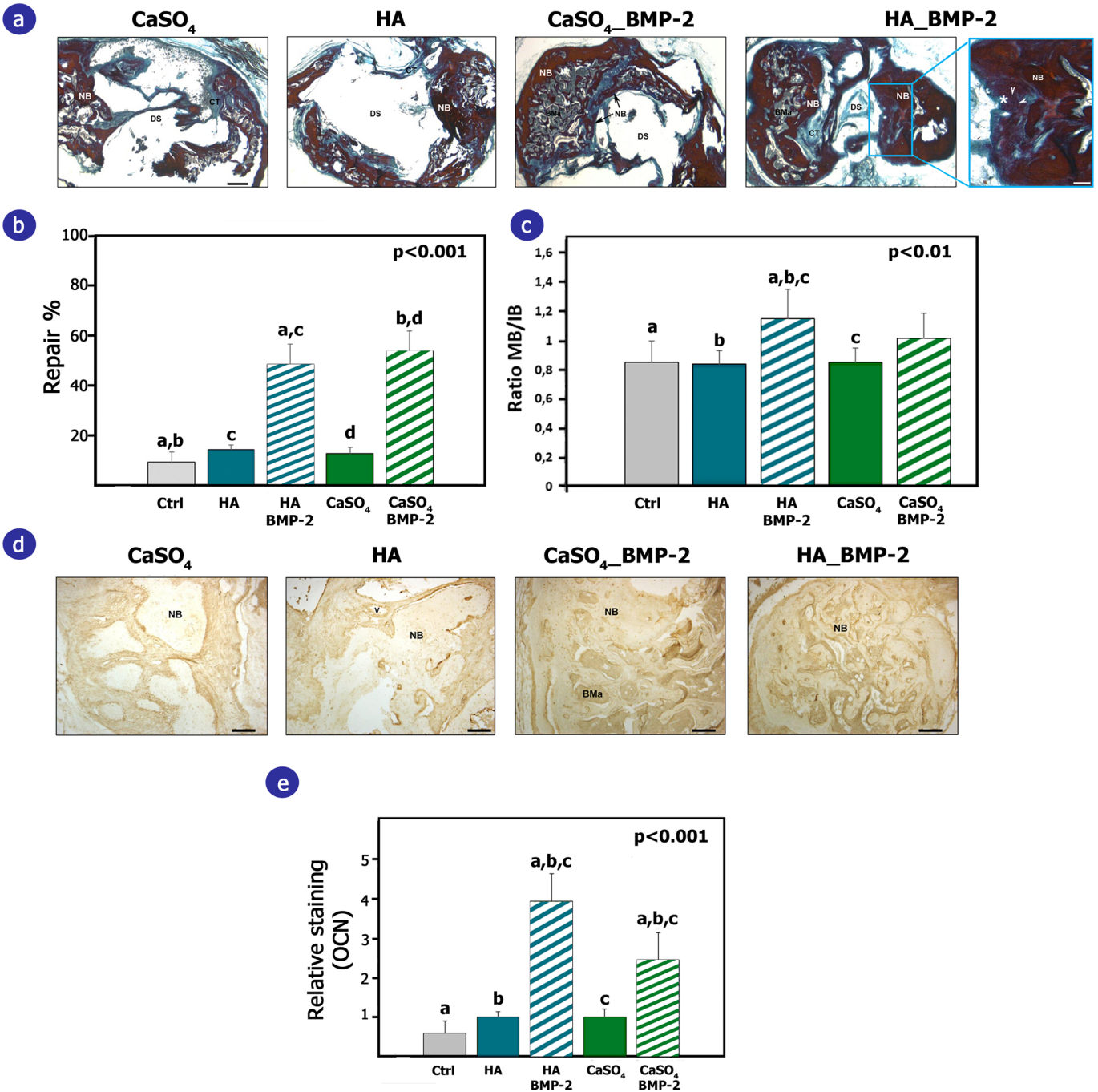
a
CaSO4
HA
CaSO4_BMP-2
HA_BMP-2
NB
CT
DS
BMa
V
b
Repair %
p<0.001
a,b
c
a,c
d
b,d
Ctrl
HA
HA BMP-2
CaSO4
CaSO4 BMP-2
c
Ratio MB/IB
p<0.01
a
b
a,b,c
c
a,b,c
d
e
Relative staining (OCN)
p<0.001

Figure 6

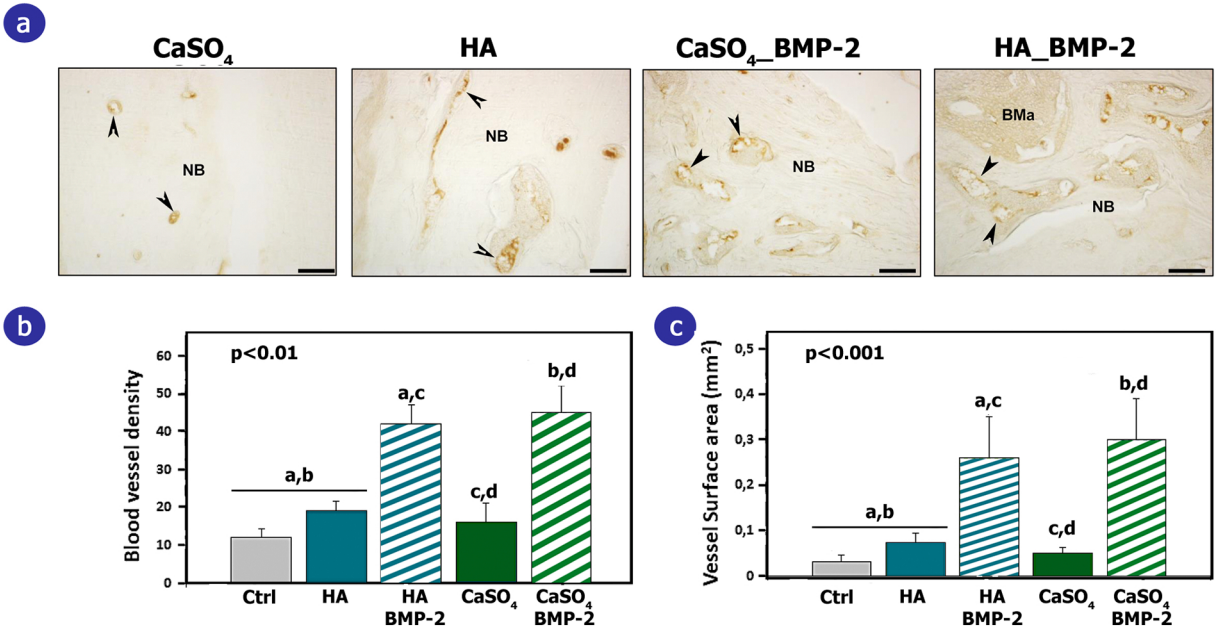
a
CaSO4
HA
CaSO4_BMP-2
HA_BMP-2
NB
NB
NB
BMa
NB
b
Blood vessel density
p<0.01
a,b
a,c
c,d
b,d
Ctrl
HA
HA BMP-2
CaSO4
CaSO4 BMP-2
c
Vessel Surface area (mm2)
p<0.001
a,b
a,c
c,d
b,d
Ctrl
HA
HA BMP-2
CaSO4
CaSO4 BMP-2

Figure 7